Marine Structures 95 (2024) 103579

Contents lists available at ScienceDirect

Marine Structures

journal homepage: www.elsevier.com/locate/marstruc

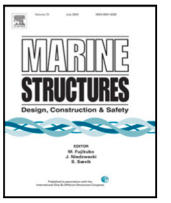

Research paper

Experimental investigation of two shared mooring configurations for a dual-spar floating offshore wind farm in irregular waves

Guodong Liang [a], Tomas Lopez-Olocco [b], Antonio Medina-Manuel [b], Leandro Antonio Saavedra-Ynocente [c], Antonio Souto-Iglesias [b], Zhiyu Jiang [a,*]

[a] Department of Engineering Sciences, University of Agder, N-4898 Grimstad, Norway
[b] CEHINAV, DACSON, ETSIN, Universidad Politécnica de Madrid, Spain
[c] Laboratorio de Dinámica del Buque, Canal de Ensayos Hidrodinámicos el Pardo (INTA-CEHIPAR), 28048 Madrid, Spain

ARTICLE INFO

Dataset link: http://canal.etsin.upm.es/papers/liangetal_sharedmooring_2023/

Keywords:
Shared mooring
Clump weight
Hydrodynamic model test
Spar floater
Floating wind farm

ABSTRACT

Shared mooring brings potential cost benefits to a floating wind farm. In such a wind farm, adjacent floaters are connected by shared lines and the total number of mooring lines is reduced. This paper presents an experimental study on a dual-spar floating offshore wind farm. In the first configuration, two spars are connected by a shared line. In the second configuration, a clump weight is added to the shared line. Irregular wave tests are performed for both configurations under operational and extreme wave conditions. The platform motions of one wind turbine and the mooring tension are measured during the tests. The influence of the added clump weight is found to be insignificant in the operational wave conditions. Under extreme waves, the added clump weight results in smaller platform motions in the wave direction and reduced tension oscillations in all mooring lines. With the additional clump weight, the extreme mooring tension in the shared line can decrease by 30% and fewer snap loading events occur, but the extreme tension in single lines can increase by 6%. This study contributes to an improved understanding of shared mooring systems and facilitates the development of model test methods for floating wind farms.

1. Introduction

A shared mooring system is an emerging concept in the design of floating offshore wind farms (FOWFs). As illustrated in Fig. 1, by connecting neighboring floating offshore wind turbines (FOWTs) with shared lines, fewer mooring lines and anchors are required for the station-keeping of an FOWF. On the other hand, coupled multibody dynamics of FOWTs result in complicated system behavior under environmental loads. Therefore, it is important to investigate the dynamic characteristics of an FOWF with shared moorings before real-life engineering applications.

In previous studies, simplified analytical models were used by Goldschmidt and Muskulus [1] to investigate the dynamics of FOWFs with shared moorings. Great cost-saving potential of the shared mooring system was reported albeit growing strength requirements with an increasing farm size. Hall and Connolly [2] studied the dynamic properties of a square-shaped semi-submersible FOWF with a shared mooring system. The individual FOWTs and mooring system were modeled in FAST [3] and MoorDyn [4], respectively. The complex restoring properties introduced by shared lines were presented together with concern for a large tendency of resonance. In a following study, Connolly and Hall [5] proposed a design algorithm based on quasi-static modeling for shared mooring systems in pilot-scale FOWFs. Different configurations of shared mooring systems were analyzed for a

* Corresponding author.
E-mail address: zhiyu.jiang@uia.no (Z. Jiang).

https://doi.org/10.1016/j.marstruc.2024.103579
Received 19 September 2023; Received in revised form 12 December 2023; Accepted 16 January 2024
Available online 30 January 2024

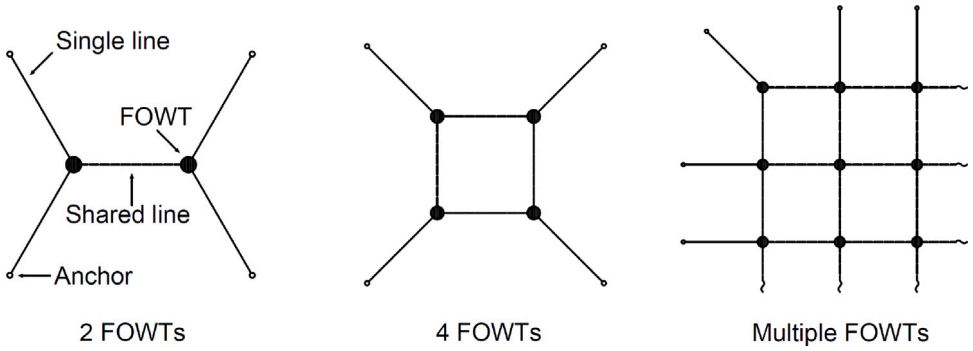

Fig. 1. Illustration of a layout pattern for FOWFs with shared mooring systems.

square-shaped four-turbine FOWF in a case study. Wilson et al. [6] carried out a design and optimization of shared mooring systems based on a linearized model for the force-horizontal displacement relationship of FOWTs. The established approach was used to analyze shared mooring systems with different farm sizes and mooring layouts. Hall et al. [7] proposed a systematic design process for a ten-turbine FOWF with shared moorings and shared anchors. The linearized model developed in Wilson et al. [6] was applied, and coupled analysis was performed in FAST.Farm [8]. The design using shared lines and shared anchors reduced the mooring installation cost by 26% compared to an FOWF with individually moored FOWTs. In the following research, a comparative study was conducted by Lozon and Hall [9] between the shared mooring system designed in [7] and the individually moored mooring system. Dynamic analysis was performed in FAST.Farm, and motions of FOWTs and structural responses were investigated. It was concluded that for that specific design case, the shared mooring system did not introduce additional dynamic response concerns.

The theory of elastic catenary of hanging cables was first applied to model the shared line by Liang et al. [10]. In a follow-up study, Liang et al. [11] studied the natural periods and natural modes of a dual-spar FOWF with a shared line by linearizing the mooring stiffness and solving the eigenvalue problem. The influence of mooring properties was investigated. The influence of aerodynamic loads on a parked dual-spar FOWF with a shared line was studied in [12]. It was found that the extreme response of the floating system was not entirely wave-dominant. In a following study [13], dynamic analyses were performed in SIMA [14,15] for the dual-spar FOWF with a shared line under extreme environmental conditions. Compared to a single FOWT, larger horizontal platform motions and higher mooring tension in single lines were observed. Loading directions showed a significant influence on dynamic responses for the specific mooring layout and mooring responses were sensitive to the shared line diameter due to variations in pretension. Recently, an innovative tethered-buoy shared mooring system was investigated for a dual-spar FOWF and compared with alternative shared mooring layouts [16]. Large mean motions were observed for the FOWTs in the tethered-buoy configuration, but a substantial decrease was observed for the mooring tension at fairleads. In these studies, simplified analytical methods and numerical modeling are the primary investigation methods for the design and analysis of FOWFs of various sizes with shared mooring. State-of-the-art mid-fidelity numerical simulation tools like FAST [3] and SIMA [14,15] were applied.

Alternatively, experimental methods by use of hydrodynamic model tests can offer additional physical insights into FOWT systems, and the test outcomes can be used for calibration or verification of numerical models. Many experimental studies can be found for individual spar-type FOWTs. In an early work, Nielsen et al. [17] performed an experimental study on a scaled Hywind spar FOWT to verify the results from two numerical tools. The Froude scaling law was applied to the physical dimensions, and a scaling ratio of 47 was adopted. Model tests were conducted under different loading conditions and good agreements were found in the comparison of wave-only test results. Duan et al. [18] conducted model tests on a scaled Hywind spar FOWT with a scaling ratio of 50. The rotor system was allowed to freely rotate, which resulted in an unmatched Reynolds number, but the agreement of the most significant aerodynamic load, the axial thrust, was maintained. Differences in the structural responses of the FOWT were observed in the presence of waves. Xu and Day [19] performed an experimental investigation of the Hywind FOWT with an emphasis on the dynamics of the motion of the mooring line. The scaling ratio was set at 74 and wave-only loading conditions were considered. During regular wave tests, snap loads were observed in mooring lines when the wave frequencies do not coincide with the heave or pitch natural frequencies of the FOWT. Besides, experimental studies are also found for FOWTs supported by different floaters, e.g. semi-submersible [20] and tension-leg platforms [21].

Despite the much existing literature on FOWT model tests, research interests are mainly focused on the design of the mooring or floater, the test methods, and the load effects of individual FOWTs. For FOWFs, there exist pilot-scale farms, e.g., Hywind Scotland [22] (in operation) and Hywind Tampen [23] (under construction), and these farms consist of individual FOWTs with separate mooring lines. So far, no literature on FOWF model tests, with or without shared moorings, has been found in the public domain. For such a model test, technical and economic challenges abound. On the one hand, many existing test facilities do not allow quality measurements, instrumentation, and placement of several FOWTs with a reasonable scale factor at an ocean basin. On the other hand, while the difference between model and prototype test cost is massive, still the construction, manufacturing, layout, and testing of a model FOWF of several FOWTs can be time-consuming and costly.

To address these challenges and to fill in the research gap of FOWFs with shared mooring systems, we selected a pilot-scale FOWF and carried out extensive model tests under various wave conditions. Wind loads acting on FOWTs are not modeled. The tested FOWF consists of two spar FOWTs located at a water depth different from that of previous numerical studies [11,13]. In

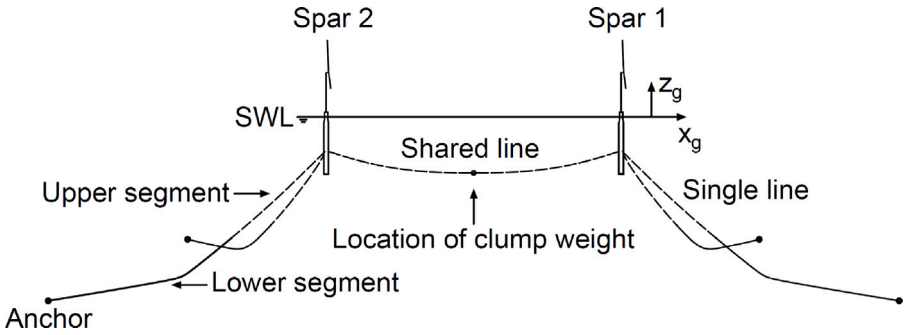

Fig. 2. Illustration of the dual-spar FOWF with shared mooring configurations (SWL: still water level, dashed line: wire, solid line: chain).

Table 1
Mooring properties of the selected single line design (full scale).

Mooring property	Chain	Wire
Material	R3 studless chain	Sheathed steel wire rope
Diameter [mm]	140	95
Sheath thickness [mm]	–	10
Mass density [kg/m]	392.00	47.39
Weight in water [N/m]	3535.94	360.42
Extensional stiffness [N]	1.53E+09	8.47E+08
Minimum breaking strength [N]	1.43E+07	9.34E+06

order to evaluate the influence of different shared line alternatives on platform motion and mooring dynamics, we considered two shared mooring configurations in the tests, i.e., the baseline configuration with a steel-wire shared line and the clump configuration with a clump weight attached to the middle of the shared line. In a previous study [13], the shared line experienced large tension variations and snap events were observed in the simulations. Lopez-Olocco et al. [24] found that by adding clump weights to single lines, the horizontal motions of a semi-submersible FOWT could be reduced. Therefore, it is of interest to investigate whether the station-keeping performance of a shared mooring system can benefit from adding clump weights to the shared lines.

Although numerical modeling offers a promising alternative, it also has limitations. The physical nonlinearities and the difficulty of properly modeling hydrodynamics response of FOWTs pose challenges for accurate simulations. Hence, it is imperative to integrate both experimental and numerical models for comprehensive and reliable predictions. Model testing remains indispensable despite challenges as it bridges the gap between theoretical predictions and real-world behaviors, paving the way for continuing growth and development in designing efficient structures and mooring systems for FOWFs.

The emphasis of this paper is laid on a comparison of the dynamic responses of the parked FOWFs with different shared mooring systems under both operational and extreme wave conditions. The major contributions of this paper are three-fold: (1) advancing the hydrodynamic model testing of multiple floating wind turbines, (2) uncovering the influence of two alternative shared mooring configurations on the response dynamics, and (3) providing a database for calibration and verification of numerical models. The paper is organized as follows: an introduction to the dual-spar FOWF is given in Section 2. Details of experimental setups are described in Section 3. Results of platform motion responses are analyzed and discussed in Section 4, followed by results of mooring responses in Section 5. Final conclusions are drawn in Section 6.

2. The prototype dual-spar FOWF

2.1. Layout and structural components of the FOWF

The dual-spar FOWF is illustrated in Fig. 2. This pilot-scale FOWF consists of two OC3 Hywind spar FOWTs [25,26] with a draft of 120 m. The FOWTs are placed in the global surge direction, i.e., along the x_g-axis. The initial turbine spacing is 750 m which is approximately six times the rotor diameter. The turbine spacing of the dual-spar FOWF is limited by the dimensions of the testing facility. In practice, the turbine spacing of FOWTs in an FOWF should be determined considering the impacts of aerodynamic interactions [27]. The water depth considered in this study is 235 m.

As shown in Fig. 2, each FOWT is moored by two single lines from the fairleads to seabed anchors. For the baseline configuration, two FOWTs are connected by a shared line at the fairleads. For the clump configuration, the mooring properties of all mooring lines are the same as those for the baseline configuration and a clump weight is attached to the mid of the shared line; see Fig. 2. The fairleads of all the mooring lines are located at 70 m below the still water level and 5.2 m away from the centerline of the corresponding FOWT [26]. The radius from the centerline of each FOWT to the corresponding anchors is 623.53 m. The projected angle between two adjacent mooring lines is 120 degrees in the horizontal plane.

Because the water depth is different from the one considered in [26], a proper redesign of single lines has been performed for a single spar FOWT for the water depth of 235 m. A two-segment design is chosen for single mooring lines because of practical

Table 2
Mooring properties of the two shared mooring configurations (full scale, refer to Fig. 2).

Mooring line	Mooring component	Parameter	Baseline	Clump
Single line	Upper segment	Property[a]	Wire	Wire
		Length [m]	250	250
	Lower segment	Property	Chain	Chain
		Length [m]	415	415
Shared line	Segment	Property	Wire	Wire
		Length [m]	739.6	739.6
	Clump weight	Submerged weight [t]	–	15

[a] Mooring properties 'Chain' and 'Wire' refer to Table 1.

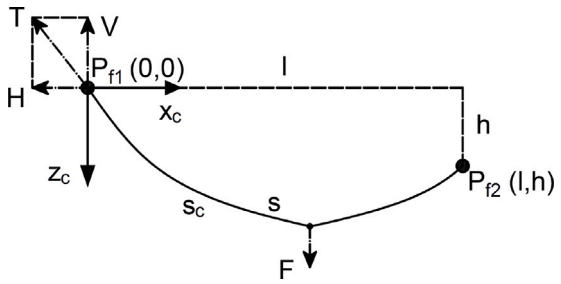

Fig. 3. Illustration of a shared line with a clump weight in the catenary plane.

considerations. Details of the design process can be found in [28]. The selected design of single lines has an upper segment made of steel wire rope and a lower segment made of chain links. Mooring properties of the selected design are summarized in Table 1. Steel wire rope is also used as the material for the shared line. Due to limited design references for shared mooring lines, the same wire properties shown in Table 1 are used for the shared line. Mooring properties of the two shared mooring configurations are listed in Table 2. As shown, the only difference between the two configurations is the clump weight.

2.2. Linearization of mooring stiffness

Considering the 6-DOF rigid body motions of two FOWTs, the general eigenvalue problem of the dual-spar FOWF can be formulated as:

$$[\boldsymbol{M} + \boldsymbol{A}(\omega)]\,\ddot{\boldsymbol{X}}(\omega) + \left[\boldsymbol{C}_{\boldsymbol{H}} + \boldsymbol{C}_{\boldsymbol{M}}\right]\boldsymbol{X}(\omega) = \boldsymbol{0} \tag{1}$$

where $\mathbf{M}$ and $\mathbf{A}(\omega)$ are the mass matrix and the frequency-dependent added mass matrix of the floating system. $\mathbf{C_H}$ and $\mathbf{C_M}$ are the hydrostatic stiffness matrix and the linearized mooring stiffness matrix, respectively. $\mathbf{X}(\omega)$ is the system state vector which describes the motions of two FOWTs in 12 DOFs. Natural frequencies and corresponding eigenmodes of the FOWF can be calculated by solving Eq. (1). As shown in [11], the coupled hydrodynamic added mass and hydrostatic stiffness matrices of the FOWF were obtained by performing hydrodynamic analyses in the frequency domain [29]. For both shared mooring configurations, a hydrodynamic analysis was performed for the panel model in which two spar floating foundations were placed apart with the initial turbine spacing (750 m). As the difference between this initial turbine spacing and the spacing after reaching a static equilibrium is less than 2% in both cases, the influence of the spar positions is minor on the results. Hence, $\mathbf{M}$, $\mathbf{A}(\omega)$ and $\mathbf{C_H}$ are the kept same for both configurations and the difference in natural frequencies results from the linearized mooring stiffness matrices.

The mooring stiffness of the FOWF was linearized about its static equilibrium position. An analytical method [11] was applied to model the two-segment single lines and the shared line. For the shared line with a clump weight, the catenary plane determined by its line shape is illustrated in Fig. 3. The origin of the coordinate system is at one fairlead, P_{f1}. The clump weight is treated as a vertical force, F, acting on the shared line. Based on Hooke's law, Newton's first law and the principle of mass conservation, a Lagrangian approach was applied to solve the asymmetrically suspended elastic catenary of a hanging cable with a point load [30]. Irvine's modeling method was applied to model the shared line with a clump weight. The nonlinear elastic catenary equations for a shared line with a clump weight are shown in Eqs. (2) and (3):

$$\begin{aligned} l = {} & \frac{Hs}{EA} + \frac{Hs}{\omega}\left[\sinh^{-1}\left(\frac{V}{H}\right) - \sinh^{-1}\left(\frac{V-F-\omega}{H}\right)\right] \\ & + \frac{Hs}{\omega}\left[\sinh^{-1}\left(\frac{V-F-\omega s_c/s}{H}\right) - \sinh^{-1}\left(\frac{V-\omega s_c/s}{H}\right)\right] \end{aligned} \tag{2}$$

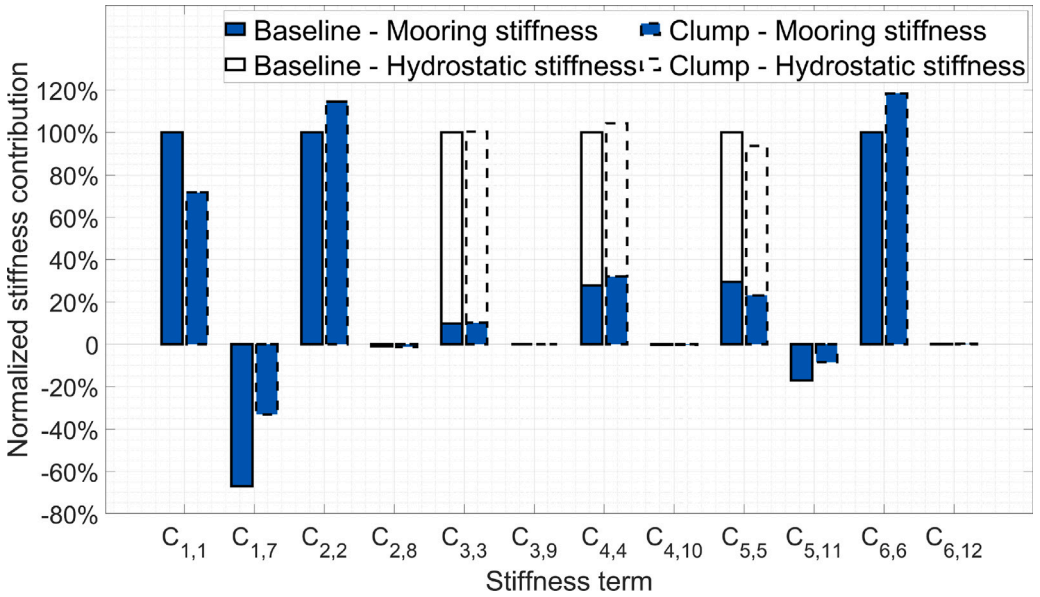

Fig. 4. Diagonal and coupled stiffness terms of the two shared mooring configurations (the stiffness term $C_{i,j}$ indicates the restoring force in the ith DOF induced by a unit displacement in the jth DOF. For each DOF, the value is normalized with regard to the corresponding total diagonal stiffness $C_{i,i}$ of the baseline configuration).

$$h = \frac{\omega s}{EA}\left(\frac{V}{\omega} - \frac{1}{2}\right) + \frac{Hs}{\omega}\left[\sqrt{1+\left(\frac{V}{H}\right)^2} - \sqrt{1+\left(\frac{V-F-\omega}{H}\right)^2}\right] + \frac{Hs}{\omega}\left[\frac{F}{H}\frac{\omega}{EA}\left(\frac{s_c}{s}-1\right) + \sqrt{1+\left(\frac{V-F-\omega s_c/s}{H}\right)^2} - \sqrt{1+\left(\frac{V-\omega s_c/s}{H}\right)^2}\right] \tag{3}$$

where l and h are the horizontal and vertical distance between two fairleads; see Fig. 3. H and V are the horizontal and vertical components of mooring tension T at the fairlead P_{f1}. s is the total unstrained length of the shared line and s_c is the distance along the shared line from P_{f1} to the point where the clump weight is attached. F is the submerged weight of the clump weight. ω is the total submerged weight of the shared line (without the clump weight). E and A are the elastic modulus and the cross-sectional area of the shared line, respectively. If the positions of two fairleads are known, the mooring tension at the fairleads can be calculated by solving Eqs. (2) and (3) numerically. With an iteration algorithm, the static configuration of the system was calculated based on mooring tension equilibrium. Starting from the static configuration, the linearized mooring stiffness was obtained by imposing a unit deflection in each DOF and calculating the resultant mooring tension.

The contributions of linearized mooring stiffness and hydrostatic stiffness in the diagonal and coupled stiffness terms of the system are presented in Fig. 4. It is found that mooring stiffness contributes most to the surge, sway and yaw DOFs [11]. The delta-line connection of the original Hywind model [31] provides yaw stiffness to the system; this is not considered in the physical modeling of the FOWTs. Therefore, the system stiffness in the yaw DOF does not have the additional yaw stiffness introduced by delta connections. The coupled stiffness between the two FOWTs arises due to the shared line. For the mooring configurations studied in this paper, platform motions in the surge and pitch DOFs bring significant changes to the tension in the shared line, therefore, mooring stiffness has noticeable contributions in the corresponding coupled stiffness; see Fig. 4. For other DOFs, the coupled stiffness is minor. The attached clump weight affects the mooring tension in the shared line and the static configuration of the FOWF. Thus, large differences in the stiffness terms of the surge, sway and yaw DOFs are observed between the two mooring configurations. As a result, the natural periods of the two configurations are expected to be different in these horizontal DOFs, as verified in Section 4.1.

3. Experimental investigation

3.1. Hydrodynamic model test

Model testing stands as a cost-effective and insightful method to predict the behavior of prototypes, especially when building the full-scale version poses risks or is economically unfeasible. It allows for preliminary performance predictions, offers substantial cost savings compared to full-scale tests, and serves as a powerful tool to calibrate numerical models.

In fluid mechanics problems, a correlation can be made from the measurements in model scale to equivalent values for a full-scale prototype if geometric, kinematic, and dynamic similarities are fulfilled. In any problem that involves waves and free surface of a fluid, inertia and gravity forces are predominant [32,33]. As a result, it is appropriate to preserve (in the model as in the full-sized

Table 3
Froude scaling of variables.

Variable	Scaling factor
Linear dimension	λ
Fluid or structure velocity	$\lambda^{1/2}$
Fluid or structure acceleration	1
Structure mass[a]	$\lambda^3 \cdot \gamma$
Structure displacement	λ
Time or period	$\lambda^{1/2}$
Force	λ^3
Moment	λ^4

[a] When scaling mass, to take into account the density difference between the sea water (SW, salt water) and the water in the ocean basin (FW, fresh water), the relation $\gamma = \frac{\rho_{sw}}{\rho_{fw}}$ is used.

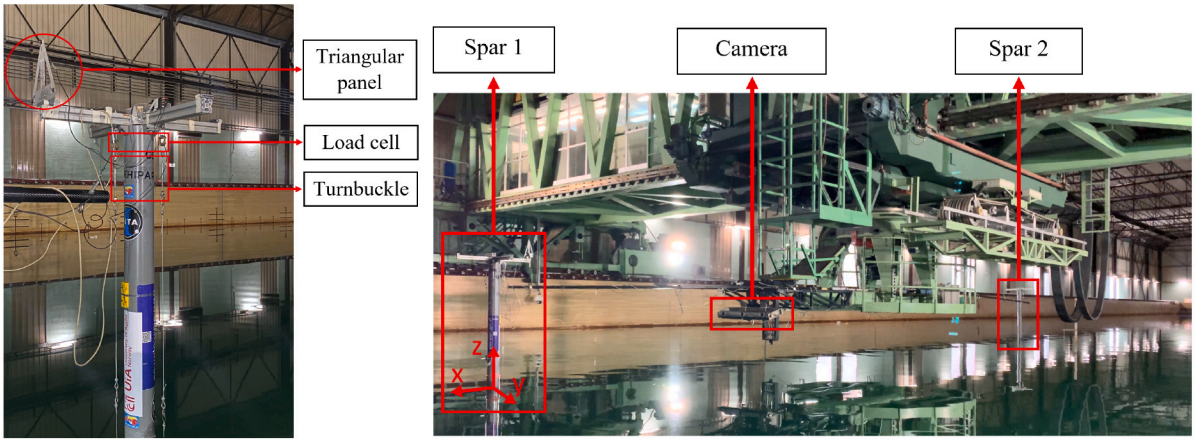

(a) Spar 1 with instrumentation (b) CPMC and two FOWT models

Fig. 5. Images of FOWT models and instrument.

prototype) the ratio of inertia and gravity forces (Eq. (4)). Therefore, in this work the Froude scaling [33] is applied and a scaling factor of $\lambda = 47$ is selected. The similarity laws for different variables used to properly model the equivalent full-sized prototype are listed in Table 3.

$$Fr = \sqrt{\frac{\text{inertia or pressure forces}}{\text{gravity forces}}} \tag{4}$$

As highlighted in this paper, the hydrodynamic model testing of moored floating platforms serves as a crucial predictive tool to understand the behavior of these structures under real-world conditions. However, the process is not without its challenges, particularly in scaling and replicating the prototype accurately.

Froude scaling, while essential in replicating gravitational effects and inertia forces, presents challenges, especially concerning hydrodynamic drag. The oversight in considering Reynolds scaling leads to inaccuracies in modeling hydrodynamic drag forces. However, it is well known that the Reynolds and Froude similitude cannot be simultaneously achieved, and allowances are made for the variation in Reynolds number. As an example, in the case of modeling mooring line drag forces, the task becomes impossible [34].

The challenge in scaling mooring lines arises when events characterized by sudden tension loss and recovery, i.e. snap/slack of the line, are present, and difficulties in modeling appear. When highly dynamic conditions are present (impulsive events), the stiffness dominates over inertia and overprediction of the forces in the model test may be encountered in these situations [35]. However, in general, the behavior of mooring lines is captured by incorporating springs into the lines.

3.2. Test facility

Model tests were conducted at the ocean basin in the *Canal de Ensayos Hidrodinámicos de el Pardo* (CEHIPAR). The length and the width of the basin are 150 m and 30 m, respectively. During the tests, the water depth of the basin was kept at 5 m. Therefore, as mentioned in Section 2, the full-scale water depth is 235 m.

A Computerized Planar Motion Carriage (CPMC) was used, which was the center of test control and data measurement; see Fig. 5(b). During the tests, the CPMC stood in the middle of two FOWT models and remained stationary. A wavemaker powered by hydraulic pumps was located at one of the 30-m sides of the basin. Waves were generated by 60 flaps of the wavemaker.

In the following sections, physical modeling of the dual-spar FOWF is described in Section 3.3. Instrumentation of the tests is briefly summarized in Section 3.4. The test program is introduced in Section 3.5.

Table 4
Target and measured mass properties of the FOWT models (model scale).

Mass property	Target value	Spar 1		Spar 2	
		Measured value	Relative difference [%]	Measured value	Relative difference [%]
Mass M [kg]	77.403	77.721	0.41	77.213	−0.25
Center of gravity COG [mm][a]	[0.0, 0.0, 893.62]	[0.002, 0.02, 890.76]	[−, −, −0.32]	[0.073, 0.00, 898.19]	[−, −, 0.51]
Moment of inertia x-axis i_{xx} [mm][b]	1029.5	1044.3	1.44	1044.3	1.44
Moment of inertia y-axis i_{yy} [mm][b]	1029.5	1044.6	1.47	1044.6	1.47
Moment of inertia z-axis i_{zz} [mm][b]	102.6	94.8	−7.60	94.8	−7.60

[a] The height of the COG is measured with regard to the keel.
[b] Moment of inertia is calculated with regard to the COG.

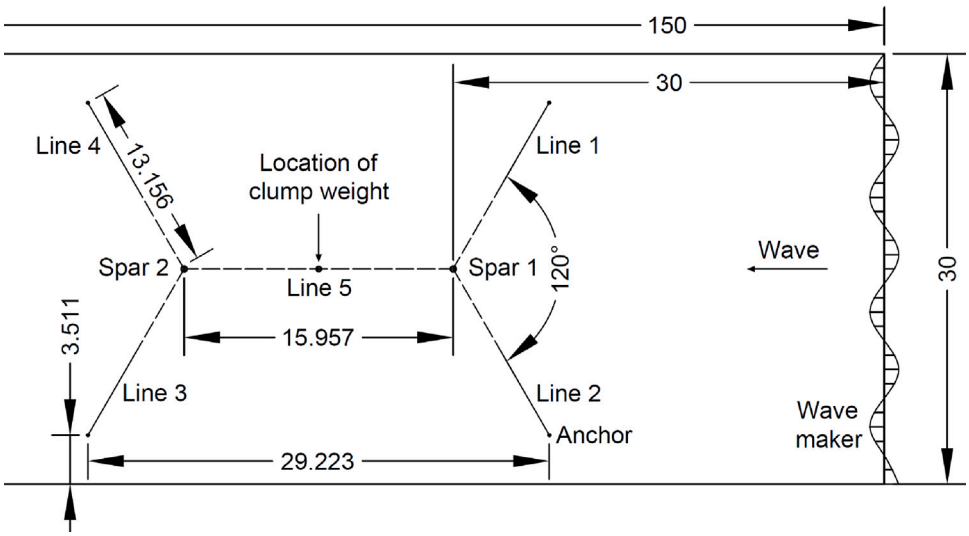

Fig. 6. Experimental layout of the dual-spar FOWF with shared mooring configurations (dimensions in [m]).

3.3. Physical modeling

3.3.1. Physical modeling of the FOWTs

Mass properties of the OC3 Hywind spar FOWT [26] were downscaled with the scaling ratio λ and taken as references to make the FOWT models. Two FOWT models were manufactured following the same process. The main body of the FOWT model is made of polyvinyl chloride. Lead panels were placed inside the spar floaters to adjust the mass properties of the model.

Because this test campaign was conducted under wave-only conditions, rotors and nacelles were not modeled. Instead, auxiliary aluminum frames were placed on top of the towers where the testing instruments were installed; see Fig. 5. Equivalent distributed weights were placed on top of the aluminum frames to adjust the inertia of the upper structure. During the manufacture, several seals were applied to the FOWT models to avoid leakage. The leakproofness of the two FOWT models was tested in the ocean basin before being towed to the test positions.

The manufacture of the FOWT models was under strict quality control. The target mass properties and the measured mass properties of the FOWT models are listed in Table 4. In general, a good agreement is achieved between the target and the measured mass properties.

3.3.2. Physical modeling of the shared mooring system

The experimental layout of the shared mooring systems is illustrated in Fig. 6. As shown, the first FOWT model, Spar 1, was placed 30 m away from the wavemaker to ensure good wave measurement qualities during the tests. For the clump configuration, a flat-cylinder clump weight was attached to the midpoint of the shared line by a diver. The submerged weight of the clump weight is 144.5 g (15 tonnes at full scale). The measured position of the clump weight on the shared line was 2.6 cm (1.22 m at full scale) from the midpoint towards the Spar 2.

The selected mooring properties in Table 1 were scaled down and taken as references in the physical modeling of mooring lines. The material of the mooring lines and the connection parts were selected to make the equivalent mass density close to the reference values. To match the material stiffness of the single lines, a set of springs (k_1) was used to connect the single lines and the anchors, as shown in Fig. 7. For the shared line, a spring (k_2) was added to the connection between Spar 2 and the shared line to achieve the equivalent material stiffness of the shared line; see Fig. 7. The resultant equivalent mooring properties in the model scale are listed in Table 5.

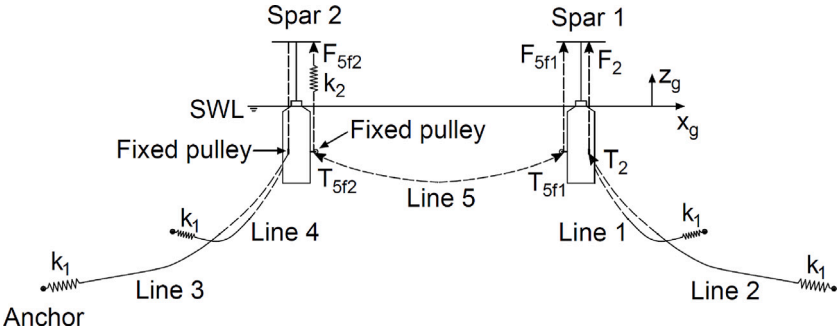

Fig. 7. Illustration of the experimental layout of the baseline configuration.

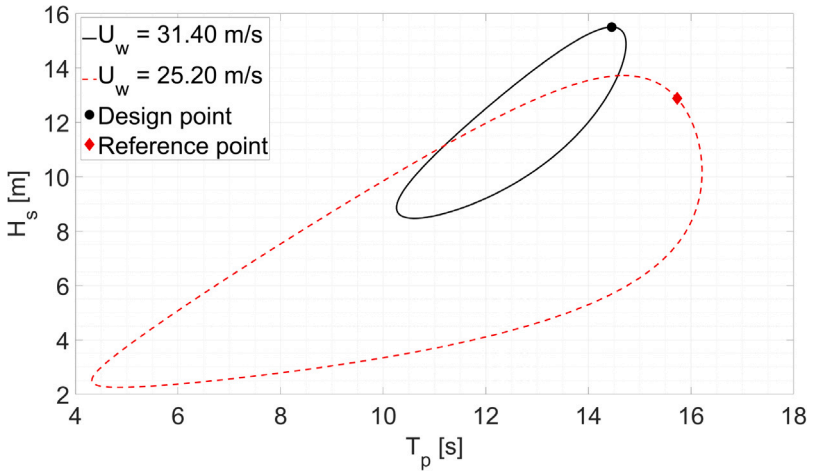

(a) 50-yr environmental contour plot

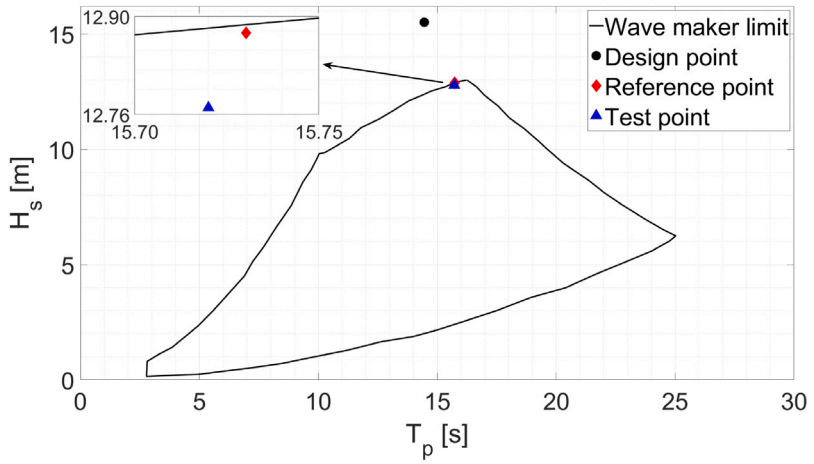

(b) Working capacity limit of the wavemaker for irregular waves

Fig. 8. Extreme sea states marked on the 50-yr environmental contour lines and the wavemaker working limit.

Load cells were used to measure mooring tension. If load cells were installed at the fairleads, they would affect the mooring angles at the fairleads due to the light weight of the mooring lines. Therefore, the load cells were installed on the aluminum frames. Fixed pulleys were mounted at the fairlead positions to transfer the mooring lines; see Fig. 7. Due to this change, the total mooring tension instead of the vertical mooring tension component was considered when tuning the mass properties of the FOWT models.

During the preparation, two FOWT models were first towed to the test positions by a small boat. Then, instruments were installed on the FOWT models. Mooring lines were set up with the aid of the diver. Anchors were placed on the bottom of the ocean basin

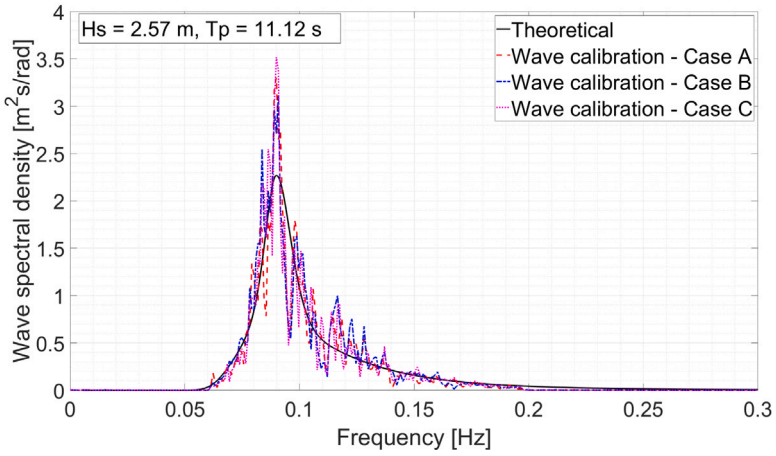

(a) Operational condition

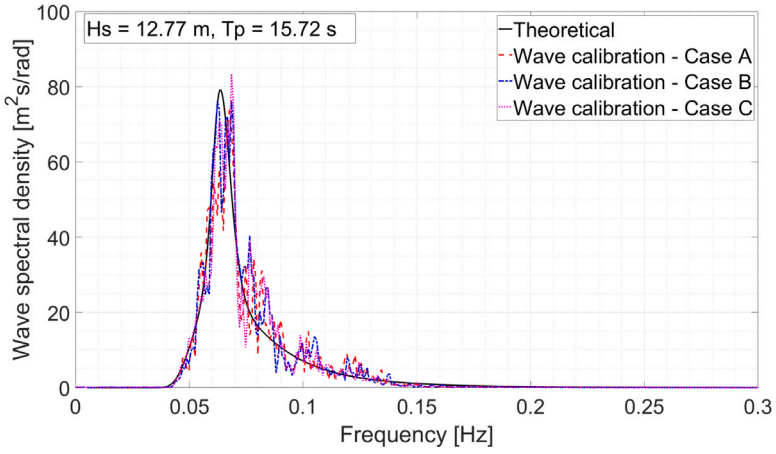

(b) Extreme condition

Fig. 9. Wave spectra of the calibrated waves.

Table 5
Mooring properties of the mooring lines used in the tests (model-scale) [28].

Mooring properties	Single line		Shared line
	Wire	Chain	
Length [m]	5.32	8.83	15.74
Mass density [kg/m]	0.02	0.16	0.02
Equivalent spring stiffness [N/m]	k_1[a] = 800		k_2[a] = 520

[a] Refer to Fig. 7 for the spring positions.

Table 6
Target and measured pretension for the two shared mooring configurations (model-scale).

Variable	Baseline			Clump		
	Target value	Measured value	Relative difference [%]	Target value	Measured value	Relative difference [%]
Pretension T_1 [N]	7.62	7.97	4.59	8.73	9.01	3.21
Pretension T_2 [N]	7.62	8.04	5.51	8.73	9.07	3.89
Pretension $T_{5/1}$ [N]	6.34	6.78	6.94	7.56	7.90	4.50
Pretension $T_{5/2}$ [N]	6.34	6.67	5.21	7.56	7.50	0.79

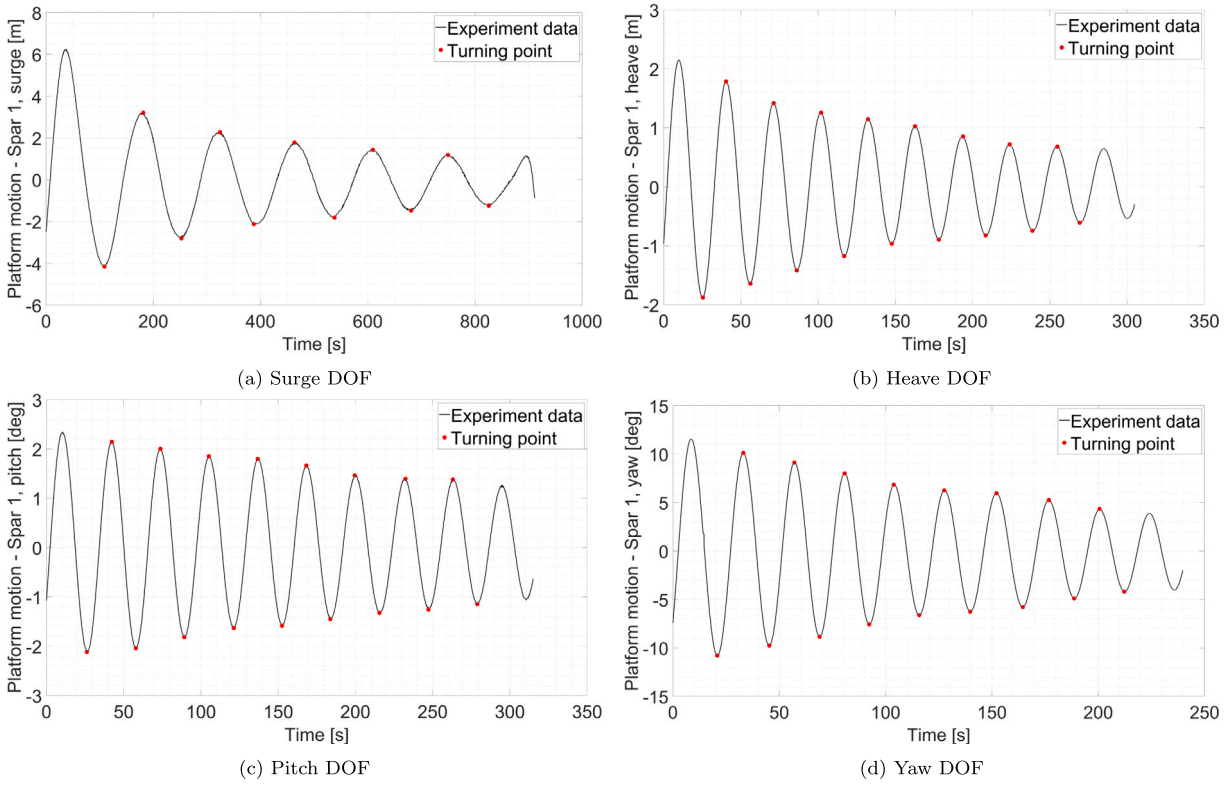

Fig. 10. Platform motions of Spar 1 in the decay test, baseline configuration.

and at exact positions shown in Fig. 6. After the setup of the mooring system, the mooring lines were checked to ensure that they were not coiled during installation. Pretension in mooring lines was measured for each configuration. The measured pretension is presented together with the target pretension in Table 6, where T_1 and T_2 indicate the mooring tension at the fairleads in Line 1 and Line 2; T_{5f1} and T_{5f2} indicate the mooring tension at the fairleads in Line 5 close to Spar 1 and Spar 2, respectively; see Fig. 7. In general, a good agreement is achieved between the target pretension and the measured pretension. With the attached clump weight, the shared line experiences a change in its shape and an increase in its pretension on static equilibrium, and the two FOWTs are drawn closer to each other. As a result, the pretension in the single lines also increases.

3.4. Instrumentation

During the model tests, variables of interest were measured by sensors and the real-time data signals were recorded with a sampling frequency of 100 Hz. Measuring sensors were installed and calibrated before the model tests.

During the tests, the absolute wave height was measured by sensors at two measurement points. The first measurement point was located below the CPMC, far enough from both FOWT models. The second measurement point was located close to Spar 2 to measure the wave field at Spar 2. The 6-DOF motions of Spar 1 were measured by an optical tracking system (KRYPTON), a camera-based dynamic position measurement system [36]. The three probes of the KRYPTON were mounted on a triangular panel and attached to the top of the aluminum frame of Spar 1, and the motions of the panel were tracked by the camera; see Fig. 5. The motions of Spar 2 were not measured during the test due to a lack of equipment.

Four one-component load cells with strain gauges were used to measure the mooring tension at the fairleads of line 1, line 2 and line 5 (both fairleads). Each upper end of the mooring lines passed through the fixed pulley at the fairlead position first, then was fixed by a turnbuckle used to adjust the pretension. The turnbuckle was linked to the load cell for tension measurement and the load cell was connected to the aluminum frame; see Fig. 5(a). The pretension of each mooring line was measured for both configurations under static equilibrium and the mooring tension due to wave loads was measured during the tests.

3.5. Test program

3.5.1. Decay tests

Decay tests were conducted for both shared mooring configurations to identify the natural periods and damping ratios of the floating system. Natural periods of a dual-spar FOWF with a shared line were studied in [11]. Considering the 6-DOF rigid body

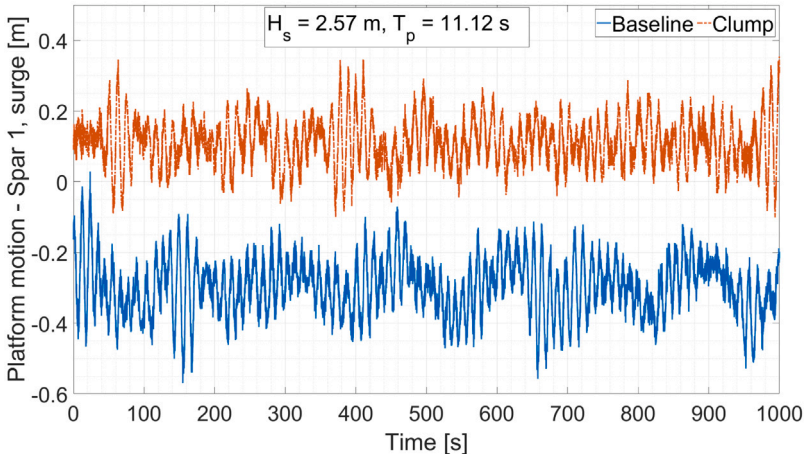

(a) Operational condition

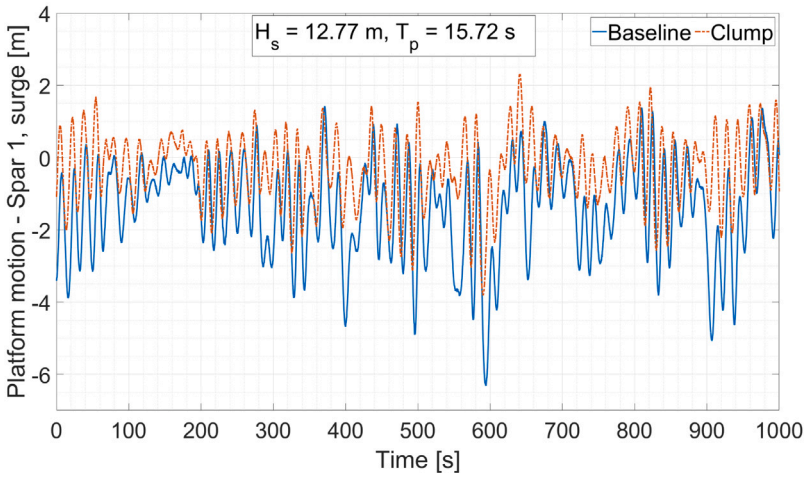

(b) Extreme condition

Fig. 11. Time series of platform surge motion — Spar 1, case C.

Table 7
Environmental parameters of the two test sea states in irregular wave tests.

Environmental parameter	Full scale		Model scale	
	Operational	Extreme	Operational	Extreme
$U_{w,Hub}$ [m/s]	11.40	–	–	–
H_s [m]	2.57	12.77	0.05	0.27
T_p [s]	11.12	15.72	1.62	2.29

motions of each FOWT, the dual-spar FOWF has twelve natural periods and eigenmodes. In these eigenmodes, two FOWTs move either in phase (Mode 1) or 180 degrees out of phase (Mode 2) in the specific DOFs. To excite these eigenmodes, initial displacements or rotations must be applied to both FOWTs. This was difficult to implement due to practical limitations. Therefore, for the free decay in translational DOFs, only Spar 1 was moved manually to get an initial displacement. For the decay in rotational DOFs, only Spar 1 was rotated manually to get an initial rotation. As a result, only six eigenmodes were excited during the decay tests and the corresponding natural periods were estimated from the results. With an initial displacement or rotation, Spar 1 was released and motions of Spar 1 were measured until the oscillation died out. For each DOF of Spar 1, the procedures were repeated three times and the initial displacements or rotations had minor differences.

3.5.2. Irregular wave tests

To characterize the dynamic behaviors of the FOWF, irregular wave tests were conducted in one operational sea state and one extreme sea state. The environmental conditions of the sea states were determined based on the joint distribution of the mean

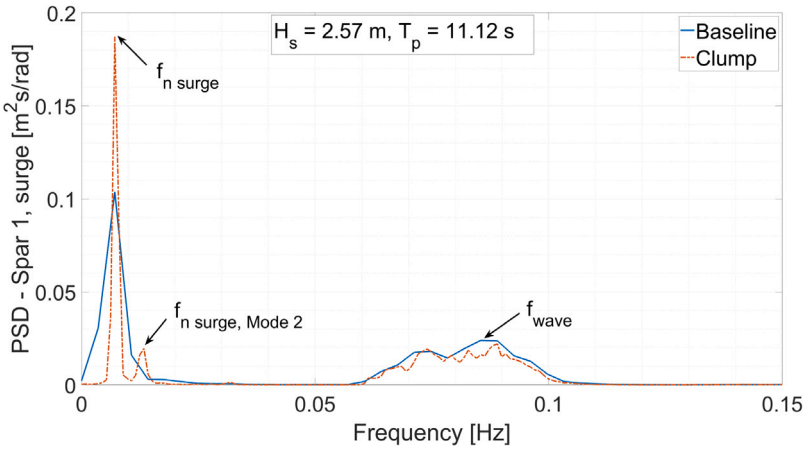

(a) Operational condition

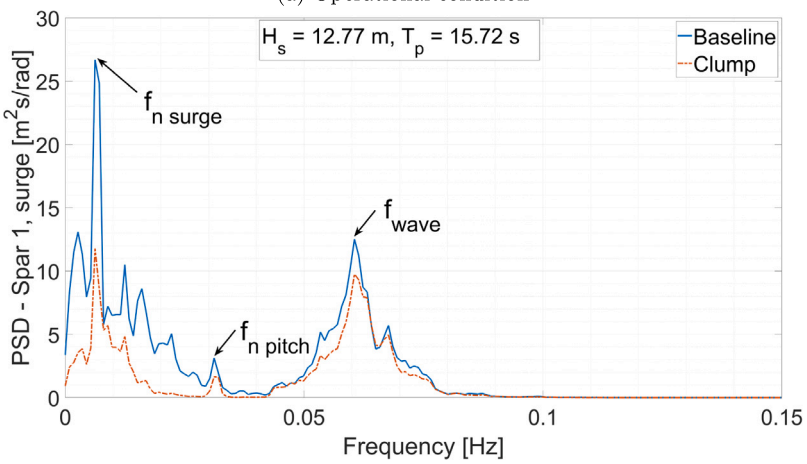

(b) Extreme condition

Fig. 12. Platform surge motion spectrum — Spar 1 (averaged over three cases).

wind speed (U_w), the significant wave height (H_s) and the spectral peak period (T_p) of a European offshore site, "Norway 5" [37], which has a water depth of 202 m. The selected sea states are described by the JONSWAP wave spectrum [38]. For the operational sea state, H_s and T_p were determined as the mean values of the conditional distributions. For the extreme sea state, the 50-year environmental contour surface was generated from the joint distribution. The sea state with the highest H_s on the surface was selected and applied in the design of single mooring lines; marked as "Design point" in Fig. 8(a). However, this extreme sea state is outside the working capacity of the wavemaker; see Fig. 8(b). Therefore, another extreme sea state was considered. This sea state is within the working capacity range of the wavemaker and has the highest H_s on the 50-year environmental contour surface; marked as "Reference point" in Fig. 8. To ensure good wave quality, a sea state close to the "Reference point" but away from the working capacity boundary of the wavemaker was selected as the extreme sea state; marked as "Test point" in Fig. 8(b). Environmental parameters of the two test sea states are summarized in Table 7. As wind loads are not considered in the model test, the scaled mean wind speed is not presented in Table 7.

During the tests, waves propagated in the global surge direction, as shown in Fig. 6. For each sea state and to reduce uncertainties, irregular wave tests were repeated three times with different random wave seeds, i.e., Case A, Case B and Case C. The duration of each irregular wave test is one hour at full scale.

Before all the tests, wave calibrations were conducted for the two sea states without the presence of the model following the recommendations by the International Towing Tank Conference (ITTC) [39,40]. The wave elevation at the position of Spar 1 (30 m away from the wavemaker) was measured. The spectra of calibrated waves in three cases are plotted against the theoretical wave spectrum in Fig. 9. For both sea states, the differences of H_s and T_p between the theoretical value and the calibration results are less than 5%, which comply with the ITTC recommendation [41].

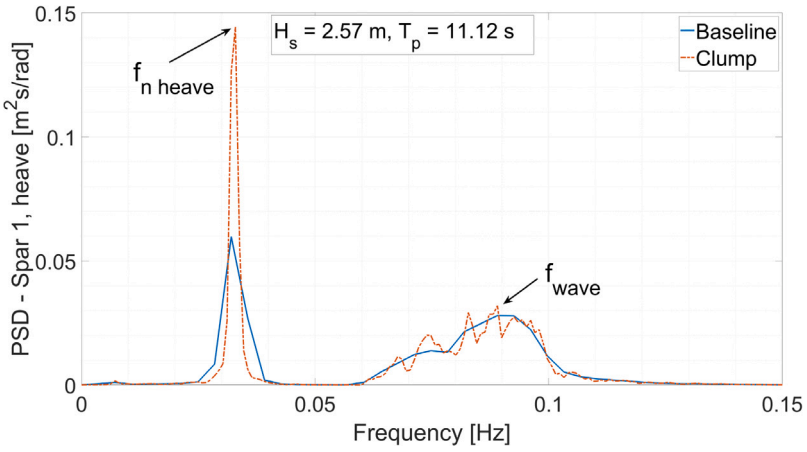

(a) Operational condition

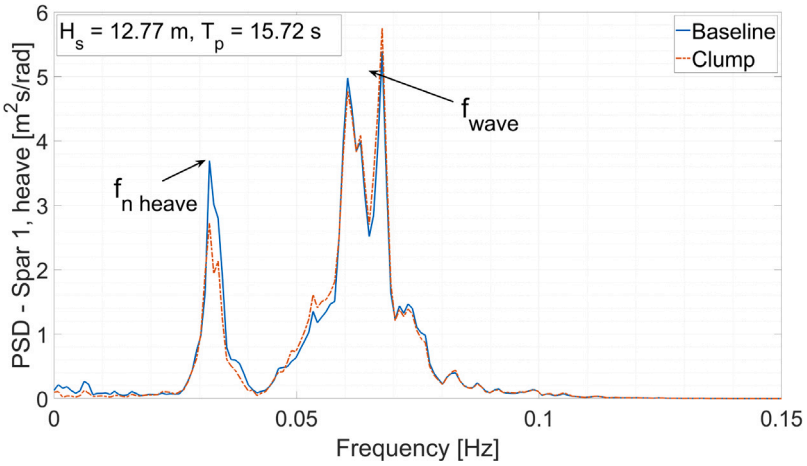

(b) Extreme condition

Fig. 13. Platform heave motion spectrum — Spar 1 (averaged over three cases).

4. Analysis of platform motion responses

The results of the spar platform motion response are analyzed and discussed in this section. As mentioned in Section 3.4, only the platform motions of Spar 1 are measured by the KRYPTON during tests. In the following sections, natural periods and damping ratios are estimated from the results of decay tests and presented in Section 4.1. For irregular wave tests, platform motion response in both operational and extreme sea states is analyzed and presented in Section 4.2. "Baseline" and "Clump" in tables and figures refer to the baseline configuration and the clump configuration described in Section 3.3.2.

4.1. Natural period and damping ratio

Platform motions of Spar 1 in decay tests were analyzed to estimate the natural periods and damping ratios of the dual-spar FOWF. Platform motions of Spar 1 in decay tests are presented in Fig. 10 for the baseline configuration. Local turning points, marked in Fig. 10, are identified from the experimental data and used in the calculation of natural periods and damping ratios. The turning point of the first peak is not used due to the transient effects. The turning point of the last peak or the turning points after ten peaks are not used due to inaccuracy.

As described in Section 3.5, for each DOF, decay tests were performed three times with different excitation displacements or rotations. Natural periods and damping ratios estimated from each test are averaged over the three records. The results are presented in Table 8. Compared with those of the baseline configuration, natural periods of the clump configuration in the surge, sway and yaw DOF decrease by 6.11%, 4.68% and 6.48%, respectively. This observation is due to the change in mooring stiffness introduced by the clump weight, as discussed in Section 2.2. Between the two mooring configurations, the differences in natural periods of other DOFs are minor because the hydrostatic stiffness dominates the total system stiffness in these DOFs. After adding the clump weight, minor changes are observed in the damping ratios of all DOFs.

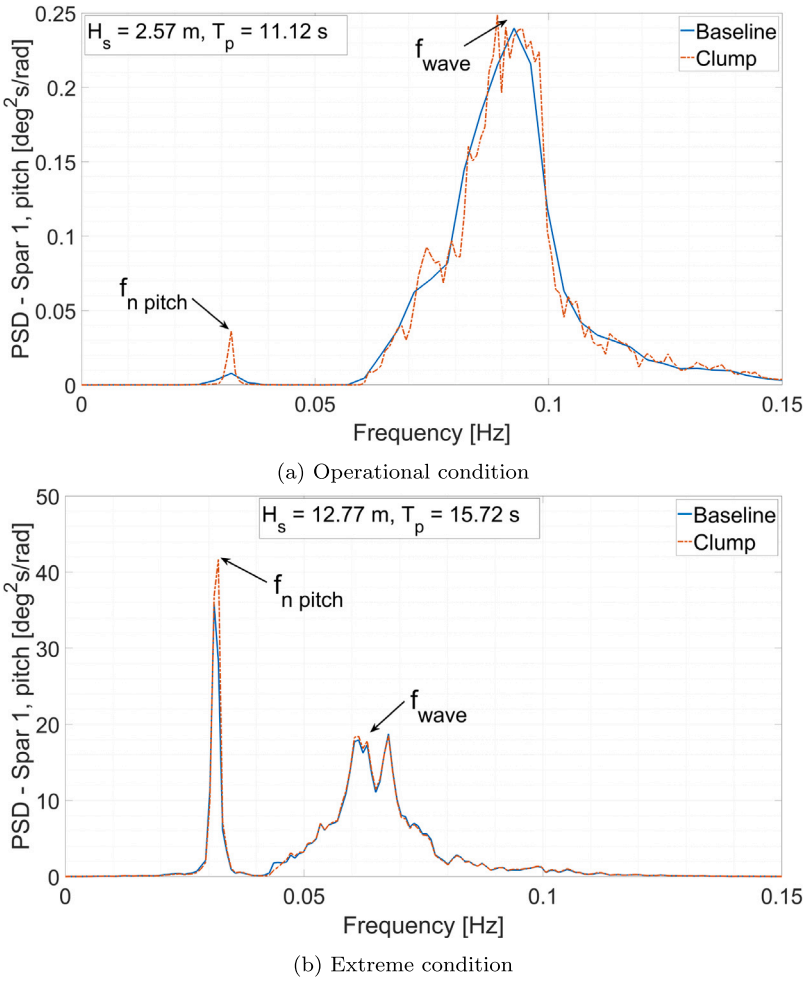

Fig. 14. Platform pitch motion spectrum — Spar 1 (averaged over three cases).

Table 8
Estimation of natural periods and damping ratios for the two mooring configurations (averaged over three tests).

Result	Configuration	Surge[a]	Sway	Heave	Roll	Pitch	Yaw
Natural period [s]	Baseline	142.88	83.89	30.50	31.56	31.62	23.93
	Clump	134.15	79.96	30.55	31.40	31.45	22.38
Damping ratio [%]	Baseline	3.56	3.02	1.86	1.08	1.32	1.83
	Clump	3.82	3.30	2.02	1.22	1.17	2.04

[a] According to [11], the large natural period in surge DOF obtained from the experimental decay test refers to Mode 1. For other DOFs, it is hard to determine whether Mode 1 or Mode 2 is excited because these two modes have close natural periods and the information of platform motion of Spar 2 is not available.

4.2. Platform motion response of Spar 1

For the irregular wave tests, the results of platform motions are investigated. The time series of platform surge motions are presented in Fig. 11 for the two wave conditions. For the operational condition, an offset is found in the mean platform surge motion between the two mooring configurations because of the difference in the static configuration. Oscillations in the surge direction around the mean positions are comparable between the two configurations. Low-frequency motions induced by wave drift forces are observed for both configurations. For floating offshore structures with large volumes, limited waterplane areas and spread mooring systems, slow-drift responses are expected [42]. From a spectral analysis, the period of this low-frequency motion corresponds to the surge eigenmode with a longer natural period in which two FOWTs move in phase. For the extreme condition, it is observed that the motion range is smaller and the oscillation is less significant for the clump configuration compared to those for the baseline configuration. This is due to the enhanced mooring stiffness introduced by the clump weight. An offset can still be observed in the mean platform surge motion between the two configurations.

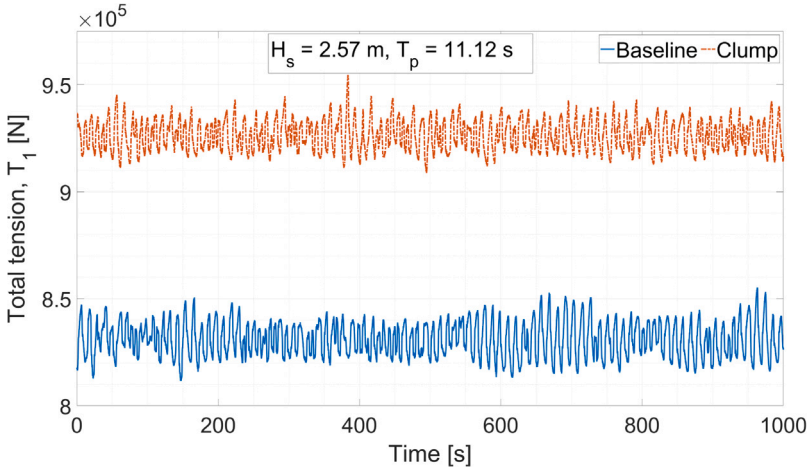

(a) Operational condition

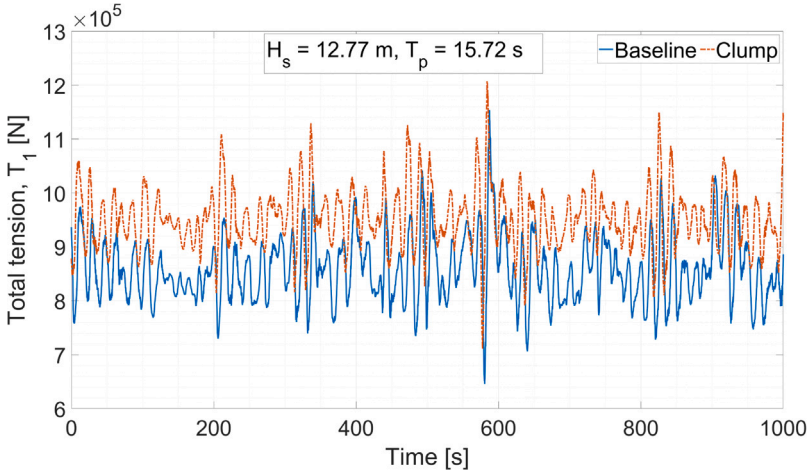

(b) Extreme condition

Fig. 15. Time series of mooring tension T_1, case C.

Table 9
Statistics of platform motion, Spar 1 in irregular wave tests (full scale, averaged over three cases).

Value	Config	Surge [m]	Sway [m]	Heave [m]	Roll [deg]	Pitch [deg]	Yaw [deg]
Operational condition							
Range[a]	Baseline	[−0.32, 0.33]	[−0.09, 0.09]	[−0.29, 0.31]	[−0.22, 0.22]	[−0.63, 0.65]	[−0.58, 0.54]
	Clump	[−0.28, 0.29]	[−0.09, 0.09]	[−0.30, 0.32]	[−0.23, 0.22]	[−0.75, 0.69]	[−0.63, 0.63]
SD	Baseline	0.09	0.03	0.09	0.07	0.19	0.17
	Clump	0.08	0.02	0.08	0.06	0.20	0.18
Extreme condition							
Range[a]	Baseline	[−5.83, 3.51]	[−0.71, 0.86]	[−2.56, 2.38]	[−1.31, 1.21]	[−5.62, 5.14]	[−13.34, 16.12]
	Clump	[−4.33, 2.81]	[−0.78, 0.82]	[−2.31, 2.45]	[−1.61, 1.29]	[−6.15, 4.84]	[−15.27, 17.05]
SD	Baseline	1.46	0.22	0.72	0.35	1.57	4.06
	Clump	1.07	0.23	0.72	0.37	1.60	4.81

[a] Motion range with regard to the mean dynamic position.

Statistics of the platform motions of Spar 1 were calculated for each case and averaged over three cases. The results are presented in Table 9. Because waves propagate in the surge direction, the influence of the clump weight on platform motions of Spar 1 is mainly reflected in the surge DOF. For other DOFs, the platform motion statistics are similar for the two mooring configurations. For the operational condition, the influence of the clump weight on the platform surge motions of Spar 1 is limited. Compared to the baseline configuration, the motion range and the standard deviation (SD) in the surge direction are slightly smaller for the clump configuration. For the extreme condition, the motion range of Spar 1 decreases by 23.55% and the SD of surge motion decreases

by 26.71% after adding the clump weight, which indicates improved station-keeping performance. For both configurations, the extreme motion ranges in the surge direction are less than 4.00% of the water depth, which is acceptable considering the design requirements of dynamic cables and farm layout [43].

In the spectral analysis, platform motion spectra are generated from platform motion time series and averaged over three cases. The averaged platform motion spectra are presented in Figs. 12 to 14 for surge, heave and pitch DOFs, respectively. As shown in the figures, for all the DOFs of interest, the platform response in the wave-frequency range is comparable between the two mooring configurations. Differences exist in the low-frequency range.

For the surge DOF, peaks with frequencies corresponding to the surge natural periods in Table 8 are identified for both configurations in addition to the response in the wave-frequency range. It is found in [11] that due to the influence of the shared line, the dual-spar FOWF with a shared line will have a lower natural period in the DOF aligned with the orientation of the shared line. A small peak is observed for the clump configuration in Fig. 12(a) which has a period of 76.58 s. This corresponds to the second surge natural period which was not captured in the decay tests. For the extreme condition, small peaks are identified for both configurations at 0.031 Hz which corresponds to the resonant motion of platform pitch. For the operational sea state, the clump configuration shows a higher peak amplitude than the baseline configuration at the surge natural frequency, whereas a lower peak amplitude is observed for the clump configuration for the extreme sea state. This difference can be explained by the mooring stiffness of the system. For the dual-spar FOWF, the mean positions of FOWTs vary significantly in different sea states and this variation results in a large difference in the system mooring stiffness [13]. The varying mooring stiffness contributes to the variation of peak amplitudes in the low-frequency range in different sea states as the amplitudes of low-frequency motions are highly dependent on the mooring stiffness [44].

For the heave and pitch DOFs, the clump configuration shows a relatively large spectral density at the peaks of the corresponding natural periods for the operation wave condition. Still, the overall amplitudes of power spectral density are small compared to those in the extreme wave condition. For the extreme wave condition, the two configurations show similar responses in the low-frequency range.

5. Analysis of mooring tension responses

The results of the mooring tension response are analyzed and discussed in this section. As introduced in Section 3.4, mooring tension at fairleads is measured for Line 1, Line 2 and Line 5 shown in Fig. 6 and indicated by T_1, T_2, T_{5f1} (fairlead on Spar 1) and T_{5f2} (fairlead on Spar 2); see Fig. 7. In the following sections, the mooring tension response of single lines is analyzed and presented in Section 5.1. The results of the mooring tension response of the shared line are discussed in Section 5.2, including an analysis of snap load events. The results of an analysis of extreme mooring tension are presented in Section 5.3.

5.1. Mooring tension response of the single lines

As mentioned in Section 3.4, the total mooring tension includes the pretension and the mooring tension induced by environmental loads. The selected time series of total mooring tension in Line 1 is presented in Fig. 15. After adding the clump weight, the mean mooring tension of Line 1 is increased by 12.38% in the operation wave condition. Similarly, an increase of 10.46% is observed in the mean mooring tension of Line 1 in the extreme sea state. The increases in the mean mooring tension of single lines are mainly caused by the difference in pretension; see Table 6.

Mooring tension statistics are calculated from time series and averaged over cases. The results of mooring tension statistics in single lines are presented in Fig. 16. For both sea states, the mooring tension statistics in Line 1 are comparable to those in Line 2 due to the symmetrical mooring layout and the 0-deg wave heading. Compared with the baseline configuration, the clump configuration has larger pretension in the single lines. Due to the added clump weight, the distance between two FOWTs under static equilibrium is smaller for the clump configuration, which means the fairleads of single lines are even further from the anchors. Therefore, pretension in single lines becomes higher for the clump configuration.

For the operational condition, the difference between the pretension and the mean tension is relatively small. This is because the mean mooring tension in the single lines is related to the mean fairlead position which is governed by the mean platform position as the spar floaters can be treated as rigid bodies. For both configurations, the mean offsets of FOWTs in the surge direction induced by the mean wave drift force are small. Therefore, the difference between the pretension and the mean mooring tension is minor. For both configurations, the SD of mooring tension in the single lines is not significant, due to the limited SD of platform motion in the surge direction; see Table 9.

For the extreme condition, the mooring tension induced by environmental loads in the single lines is higher for the baseline configuration than for the clump configuration. For example, for Line 1, the mooring tension induced by environmental loads takes 4.59% of the mean mooring tension in the baseline configuration and takes 2.12% of the mean mooring tension in the clump configuration. Besides the larger pretension in the clump configuration, the enhanced mooring stiffness also contributes to the smaller mooring tension induced by environmental loads. Though the pretension and the mean mooring tension in single lines are higher in the clump configuration, the SD of mooring tension is 6.12% lower in Line 1 and 8.57% lower in Line 2 compared to the baseline configuration. This is in line with the SD of platform surge motion shown in Table 9.

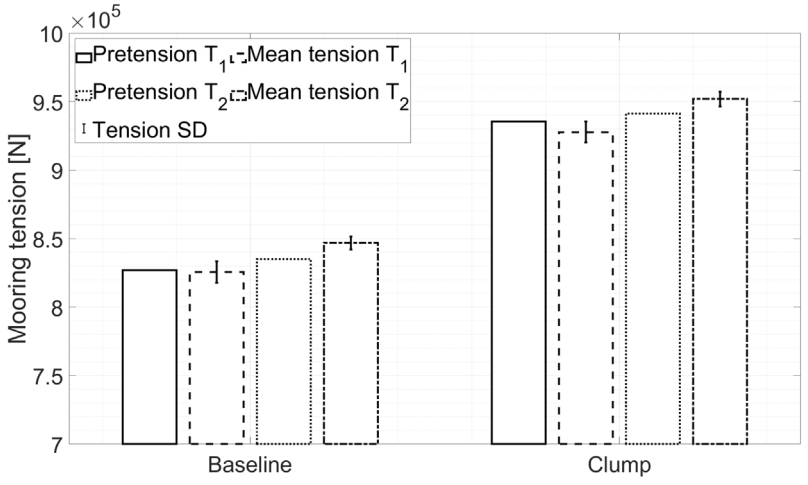

(a) Operational condition

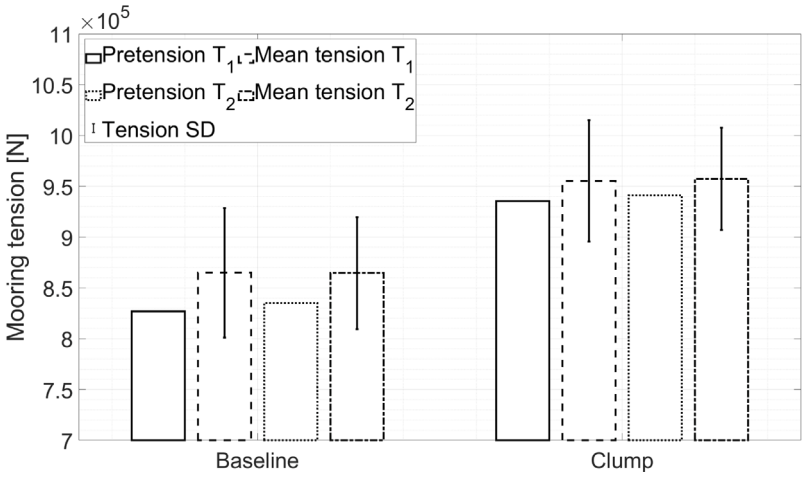

(b) Extreme condition

Fig. 16. Statistics of mooring tension of single lines (averaged over three cases).

5.2. Mooring tension response of the shared line

5.2.1. Response statistics of the shared line

Selected time series of mooring tension in the shared line, at the fairlead close to Spar 1 is presented in Fig. 17. For the operation condition, the mooring tension of the clump configuration has a higher mean mooring tension than that of the baseline configuration due to the added clump weight. But apparently, the variation of mooring tension is more significant for the baseline configuration. A similar trend is also observed in the extreme condition. As shown in Fig. 17(b), the oscillation of mooring tension is stronger for the baseline configuration than for the clump configuration. The variation of mooring tension in the shard line relates to the relative motions between the two fairleads of the shared line. From the motion ranges presented in Table 9, it can be seen that the relative motions between the two FOWTs become moderately reduced in both wave conditions for the clump configuration.

The statistics of mooring tension in the shared line are averaged over three cases. The results are plotted in Fig. 18. As discussed in Section 3.3.2, the pretension in the shared line is higher for the clump configuration than the one for the baseline configuration due to the attached clump weight.

For the operational condition, similar to that of the single lines, the difference between the pretension and the mean tension of the shared line is small due to the moderate mean platform offset in the surge direction. The SD of shared mooring tension is larger for the baseline configuration than for the clump configuration, as shown in Fig. 17(a). This could be caused by the different mooring line dynamics resulting from different shared line configurations and different mean turbine spacing, though the SD of platform motion in the surge direction is comparable for the two mooring configurations from Table 9.

For the extreme condition, the mooring tension induced by the mean wave loads is minor compared to the pretension. However, the SD of mooring tension in the shared line is significant compared to the mean mooring tension. The relative motions between

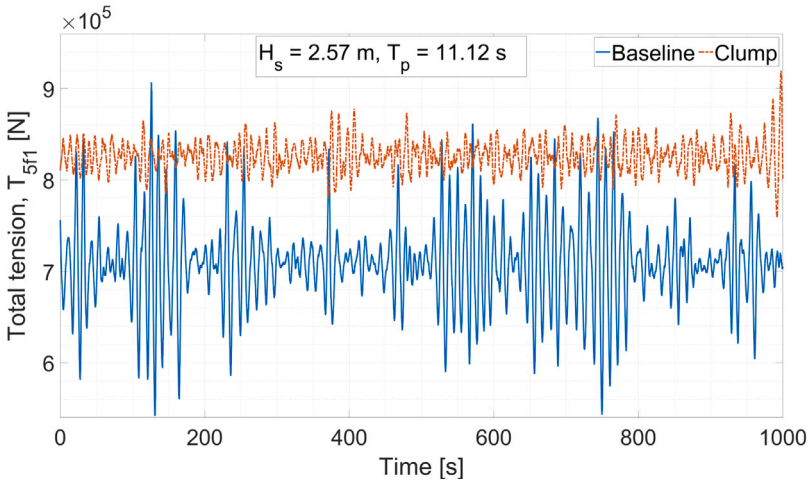

(a) Operational condition

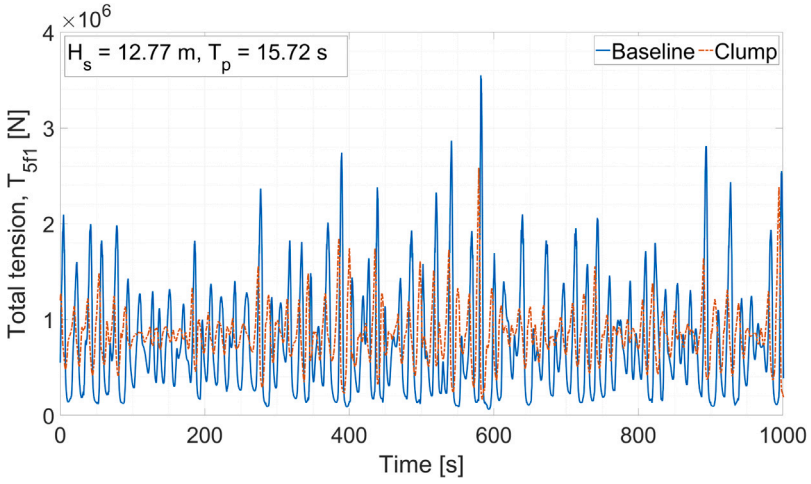

(b) Extreme condition

Fig. 17. Time series of mooring tension T_{5f1}, case C.

two FOWTs tighten and slacken the shared line repeatedly. This results in large oscillations in the shared line tension. The SD of mooring tension decreases after adding the clump weight. For the shared mooring tension T_{5f1}, the ratio between the SD of mooring tension and the mean mooring tension is 78.20% for the baseline configuration and 34.18% for the clump configuration. As shown in Table 9, the decrease of SD of platform surge motions after adding the clump weight contributes to the difference in the SD of mooring tension.

5.2.2. Snap events under extreme condition

A sharp tension spike in the mooring line after a temporary slackness is described as a snap event [45]. Considering the large relative motions between FOWTs, snap loads are of interest to be investigated for shared lines. According to [45], the mooring tension of the spike and the slackness in a snap event must fulfill the following criteria:

$$T_{slack} \leq 0.1 \cdot T_{mean} \tag{5}$$

$$T_{spike} \geq 1.9 \cdot T_{mean} \tag{6}$$

where T_{slack} is the local tension minima as the start of a snap event; T_{spike} is the local tension maxima as the end of a snap event; T_{mean} is the mean mooring tension with contributions from both pretension and the mooring tension caused by mean environmental loads.

For both the operational and the extreme conditions, time series of four mooring tension variables measured in the irregular wave tests was analyzed to identify the snap load events. From the results, snap events are only found in the shared line tension (T_{5f1}

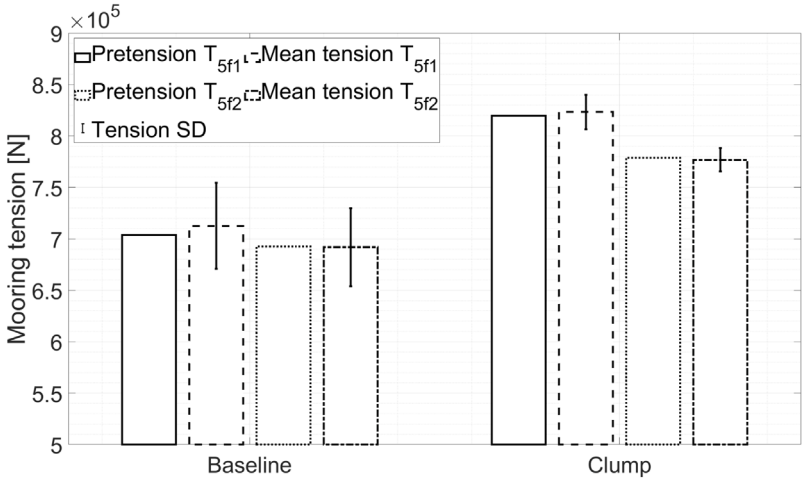

(a) Operational condition

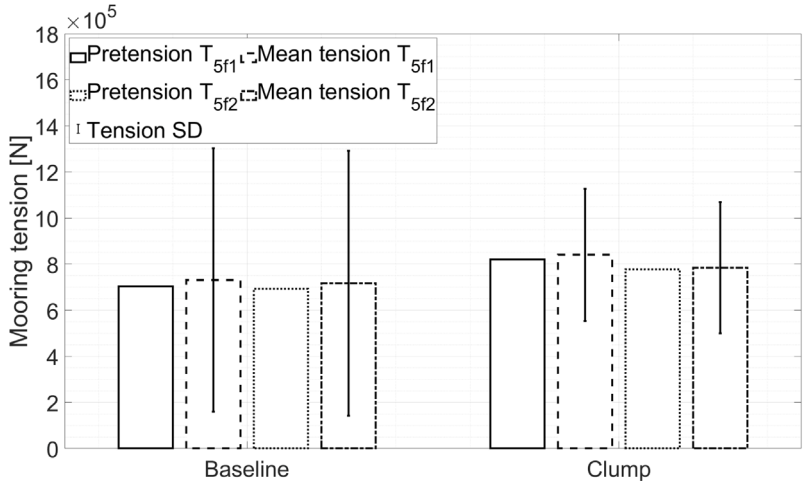

(b) Extreme condition

Fig. 18. Statistics of mooring tension of the shared line (averaged over three cases).

and T_{5f2}) under the extreme condition. The identified snap events are plotted in Fig. 19 for T_{5f2} in Case A. From the results, the number of snap events observed in the shared line decreases significantly after adding the clump weight. For example, the averaged number of snap events observed in T_{5f2} is 18.33 for the baseline configuration and 1.33 for the clump configuration. This is due to the smaller SD of mooring tension in the clump configuration, as shown in Fig. 18(b). It is concluded that adding a clump weight to the shared line may diminish the impact of snap loads and therefore, reduce the safety margin preserved for the snap loads and lead to a more cost-effective design of shared lines.

5.3. Analysis of extreme mooring tension

The extreme mooring tension is an important metric for mooring design based on ultimate limit state assessment of FOWT structures according to existing design guidelines [44,46,47]. An analysis of extreme mooring tension is performed based on the mooring tension measured in the irregular wave tests under the extreme condition. First, local tension maxima are identified according to the definition in the design standard [46] from the mooring tension time series. The identified local tension maxima in T_{5f1} are presented in Fig. 20 for case A in both mooring configurations. Then the identified local tension maxima are fitted to a three-parameter Weibull distribution [46]:

$$F(T_{max}) = 1 - \mathrm{e}^{-\left(\frac{T_{max}-\gamma}{\alpha}\right)^{\beta}} \tag{7}$$

where α, β and γ are the scale, shape and position parameters, respectively. Probability papers are generated for the fitted distributions. Examples are presented in Fig. 21 for the local tension maxima identified in Fig. 20. The most probable maxima extreme

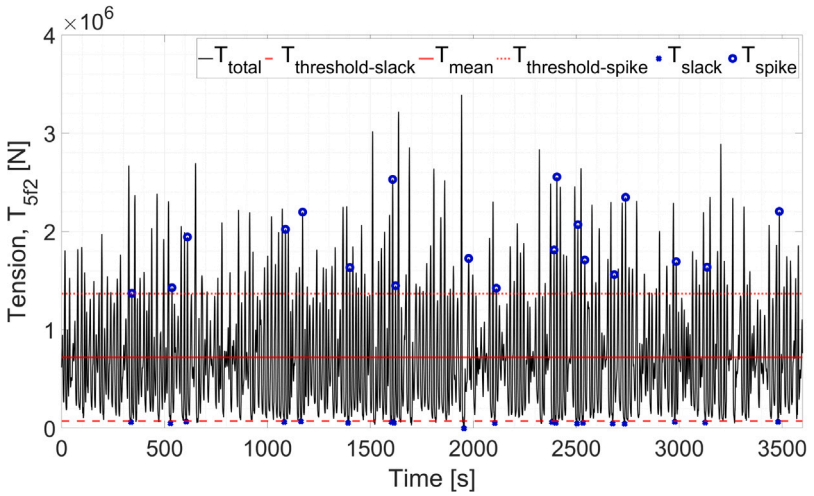

(a) Baseline configuration

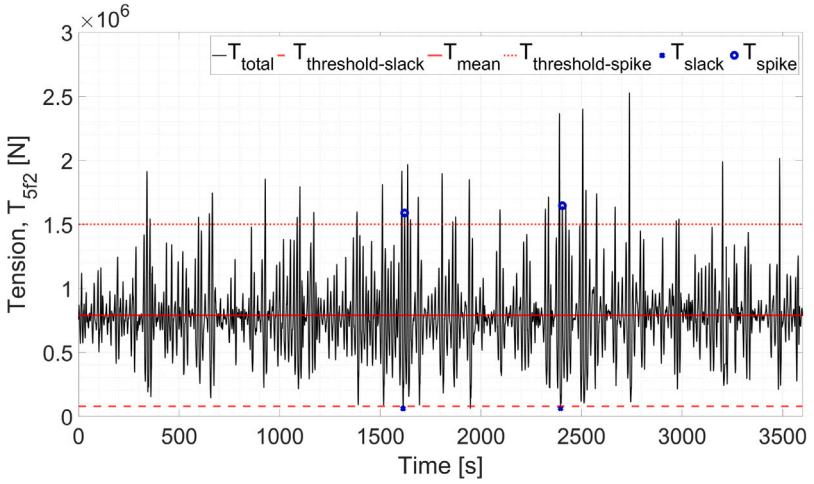

(b) Clump configuration

Fig. 19. Identified snap load events in the time series of mooring tension T_{5f2}, extreme condition, case A.

Table 10
T_{MPME} for the two mooring configurations [N] (averaged over three cases).

Configuration	T_1	T_2	T_{5f1}	T_{5f2}
Baseline	1.18E+06	1.13E+06	3.71E+06	3.66E+06
Clump	1.25E+06	1.18E+06	2.65E+06	2.55E+06

(MPME) of mooring tension can be used as a statistical reference value and is calculated based on the fitted distribution [46,48]:

$$T_{MPME} = \gamma + \alpha \left[-\ln\left(\frac{1}{N}\right)\right]^{\frac{1}{\beta}} \tag{8}$$

where N is the number of local tension maxima. For each case in the extreme condition, T_{MPME} are calculated for mooring tension variables measured during the tests. As an example, Fig. 22 shows the probability of exceedance (POE) of local maxima in the fairlead tensions T_1 and T_{5f1} in the extreme condition, Case A. The calculated T_{MPME} is also marked in the figure. As shown in Fig. 22(a), for the fairlead tension in the single line, the addition of the clumped weight increases the peak events in the time history and results in a small increment in the POE for a given level of tension threshold due to the higher pretension. For the fairlead tension in the shared line, the addition of the clumped weight reduces the peak events in the time history and results in a considerable reduction in the POE for a given level of tension threshold; see Fig. 22(b).

The averaged T_{MPME} of the three cases are presented in Table 10. By adding the clump weight, the extreme mooring tension in single lines increases by 5.93% and 4.42% and the extreme mooring tension in the shared line decreases by 28.57% and 30.33%.

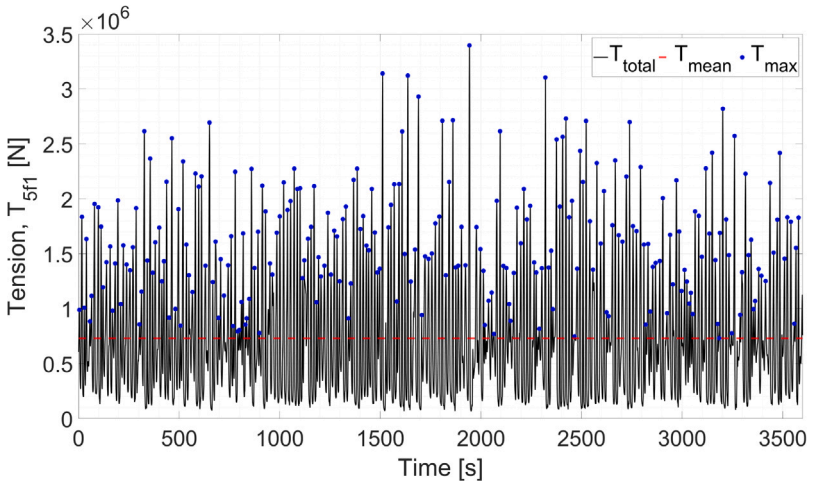

(a) Baseline configuration

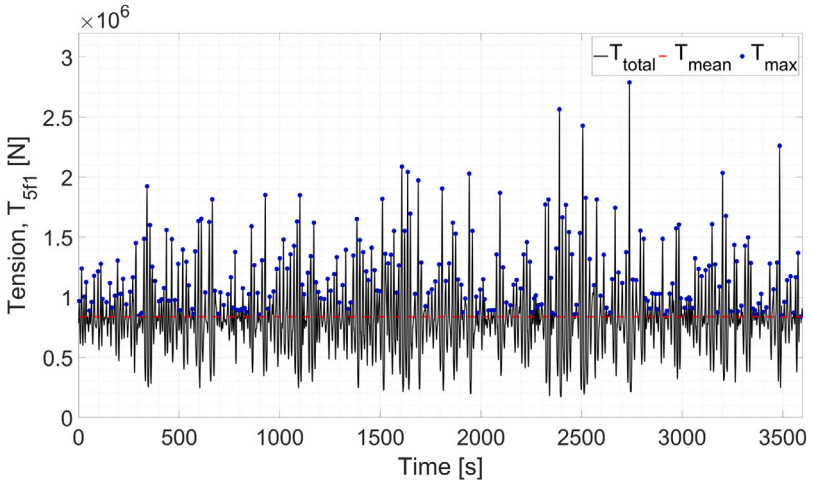

(b) Clump configuration

Fig. 20. Identified local tension maxima in the time series of mooring tension T_{5f1}, extreme condition, case A.

Since the mooring properties of the shared line are the same for both shared mooring configurations, adding a clump weight can reduce the extreme mooring tension in the shared line and lead to a lower utilization factor, which means there is a possibility of cost reduction through a redesign of the shared line.

6. Conclusion

In this paper, comprehensive outcomes of a model test campaign are presented. Hydrodynamic model tests were carried out for a dual-spar floating offshore wind farm (FOWF) with two shared mooring configurations. In the baseline configuration, two spar floating offshore wind turbines (FOWTs) are connected by a shared line. In the clump configuration, a clump weight is added to the shared line. The mooring system of the FOWF, design of the experiment, physical modeling of the structural system, instrumentation, and test program are documented in detail. From the tests, platform motions of one spar FOWT and mooring tension in the single lines and the shared line are analyzed. The results and discussions focus on the comparison of the two mooring configurations. The main conclusions are listed as follows:

- For the natural periods, the influence of the attached clump weight on the shared line is mainly reflected in the horizontal degrees of freedom (DOFs), i.e., surge, sway and yaw. This is because the diagonal stiffness terms of these horizontal DOFs only have contributions from mooring stiffness. For the other DOFs, the hydrostatic stiffness dominates in the total stiffness and therefore, the influence of the clump weight is minor. For the two configurations investigated in this study, the surge natural period decreases by 6.11% and the sway natural period decreases by 4.68% after adding the clump weight. The change in system natural periods introduced by mooring components should be considered in the design of shared mooring systems.

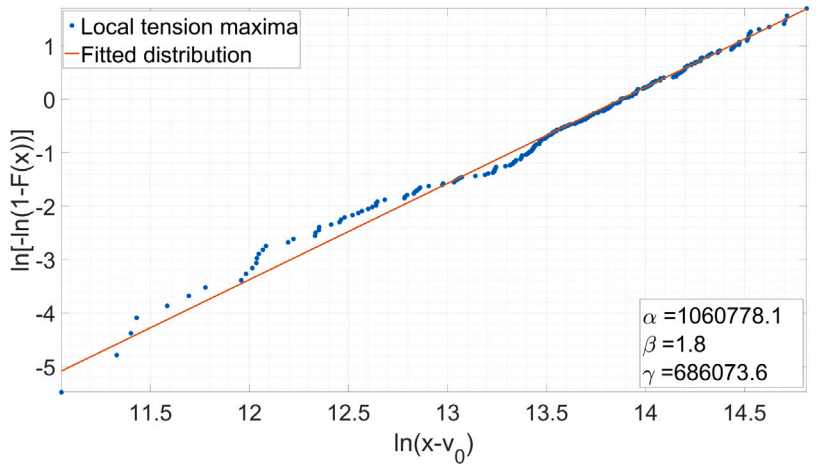

(a) Baseline configuration

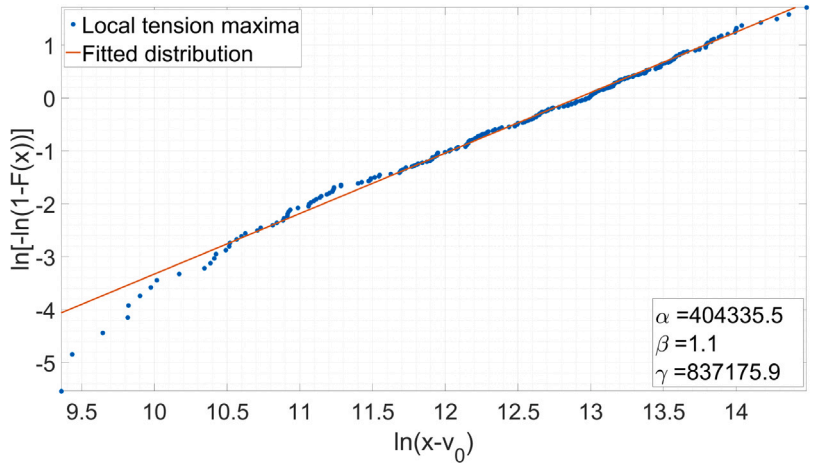

(b) Clump configuration

Fig. 21. Weibull probability papers for the fitted distribution in mooring tension T_{5f1}, extreme condition, case A.

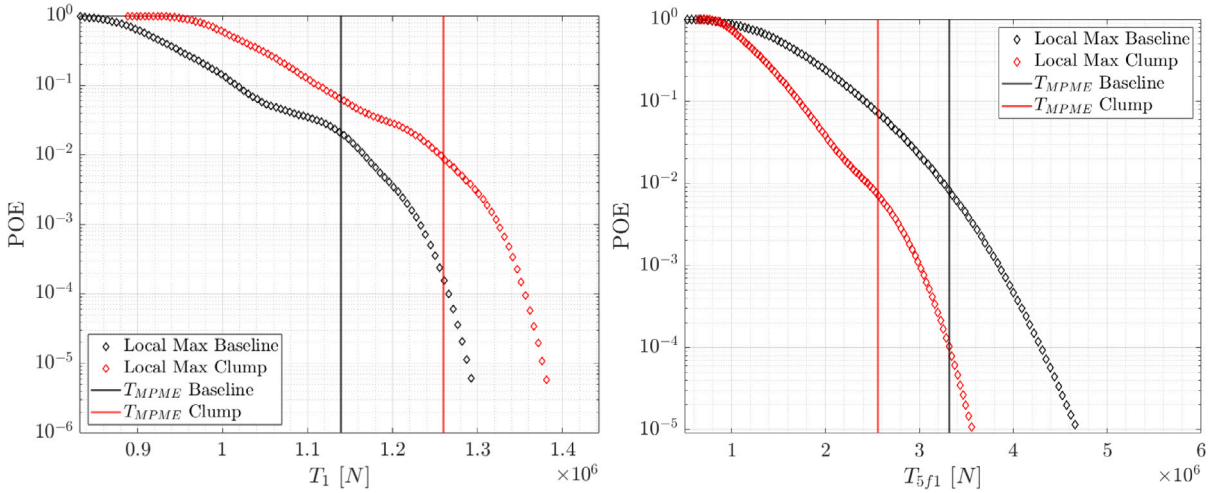

(a) T_1 (b) T_{5f1}

Fig. 22. Comparison of estimated MPME of mooring tension in the two mooring configurations, extreme condition, case A.

- In the irregular wave tests, waves propagated in the surge direction. The influence of the clump weight on the shared line is observed in the surge platform motion of Spar 1. Compared with that of the baseline configuration, Spar 1 experiences less oscillation around the mean position for the clump configuration under the extreme wave condition. This can be due to the reduced effects of low-frequency motions.
- The added clump weight increases the self weight of the shared line and drives the two FOWTs closer to each other upon the static equilibrium. Therefore, compared with the baseline configuration, the clump configuration has higher pretension in the single lines and the shared linen. The influence of the clump weight on the mooring responses is more appreciated under the extreme wave condition than under the operational condition. Both the single lines and the shared line experience lower dynamic tension in the clump configuration. Therefore, for the design of a shared mooring system, clump weights could be an option to reduce mooring tension oscillations and fatigue problems.
- Compared with those of the baseline configuration, single lines of the clump configuration have larger extreme mooring tension due to larger pretension. Therefore, if the original design of single lines does not have a sufficient safety margin, a redesign is necessary if considering adding clump weights to the shared line. For the shared line, extreme mooring tension in the shared line decreases up to 30.33% and fewer snap events are experienced by the shared line for the clump configuration. These observations indicate the potential load mitigation benefits of clump weights in the shared line design.

7. Limitations and future work

This experimental study has its limitations. Only wave conditions are considered without other environmental effects, wind, and currents. In the future, it will be interesting to study the behavior of floating wind farms with alternative mooring systems under combined loading. To achieve a better understanding of the system, more variables can be measured during the tests, e.g., platform motions of all FOWTs, mooring angles and motion of the clump weight (sagging depth). For the decay tests, more information about natural periods and eigenmodes of the coupled floating system may be obtained if both FOWTs can be excited.

The focus of this paper is on the analysis of the dynamic response of two alternative shared mooring configurations for a floating wind farm based on model test results. Based on the present physical test results, calibration and verification of numerical models and design optimization of shared mooring systems will be addressed in future work.

Interested readers can access the publicly available database to calibrate or verify numerical models in aero-hydro-servo-elastic codes. Challenges may include calibration of the drag coefficients of the submerged spar and mooring lines under varying Reynolds and Keulegan–Carpenter numbers during irregular waves.

CRediT authorship contribution statement

Guodong Liang: Data curation, Formal analysis, Investigation, Methodology, Writing – original draft, Writing – review & editing. **Tomas Lopez-Olocco:** Data curation, Formal analysis, Investigation, Methodology, Writing – review & editing. **Antonio Medina-Manuel:** Data curation, Investigation. **Leandro Antonio Saavedra-Ynocente:** Data curation, Investigation. **Antonio Souto-Iglesias:** Conceptualization, Funding acquisition, Supervision, Writing – review & editing, Resources. **Zhiyu Jiang:** Conceptualization, Funding acquisition, Investigation, Methodology, Resources, Supervision, Writing – original draft, Writing – review & editing.

Declaration of competing interest

The authors declare that they have no known competing financial interests or personal relationships that could have appeared to influence the work reported in this paper.

Data availability

The dataset used in the present study is made available on the server of CEHINAV Research Group (http://canal.etsin.upm.es/papers/liangetal_sharedmooring_2023/).

Acknowledgments

The financial supports from UH-nett Vest (Project No. 720025) and from the Norwegian Ministry of Education and Research are gratefully acknowledged. This research has also been partially funded by the Ministry of Science and Innovation of Spain through projects FOWT-DAMP2 (References: PID2021-123437OB-C21, FOWT-PLATE-MOOR and TED2021-130951B-I00). Thanks are extended to Dr. Carlos Lopez-Pavon from COREMARINE SOLUTIONS, Spain for fruitful discussions leading to the definition of some parameters of the tested configurations.

References

[1] Goldschmidt M, Muskulus M. Coupled mooring systems for floating wind farms. Energy Procedia 2015;80:255–62.
[2] Hall M, Connolly P. Coupled dynamics modelling of a floating wind farm with shared mooring lines. In: ASME 2018 37th international conference on ocean, offshore and arctic engineering. Madrid, Spain: American Society of Mechanical Engineers; 2018.
[3] Jonkman JM, Buhl ML. FAST user's guide. Golden, CO, USA: National Renewable Energy Laboratory; 2005.
[4] Hall M. MoorDyn user's guide, vol. 15, Orono, ME, USA: Department of Mechanical Engineering, University of Maine; 2015.
[5] Connolly P, Hall M. Comparison of pilot-scale floating offshore wind farms with shared moorings. Ocean Eng 2019;171:172–80.
[6] Wilson S, Hall M, Housner S, Sirnivas S. Linearized modeling and optimization of shared mooring systems. Ocean Eng 2021;241:110009.
[7] Hall M, Lozon E, Housner S, Sirnivas S. Design and analysis of a ten-turbine floating wind farm with shared mooring lines. In: Journal of physics: Conference series. volume 2362, IOP Publishing; 2022, 012016.
[8] Jonkman JM, Shaler K. FAST.Farm user's guide and theory manual. Golden, CO, USA: National Renewable Energy Laboratory; 2021.
[9] Lozon E, Hall M. Coupled loads analysis of a novel shared-mooring floating wind farm. Appl Energy 2023;332:120513.
[10] Liang G, Merz K, Jiang Z. Modeling of a shared mooring system for a dual-spar configuration. In: International conference on offshore mechanics and arctic engineering. American Society of Mechanical Engineers; 2020.
[11] Liang G, Jiang Z, Merz K. Mooring analysis of a dual-spar floating wind farm with a shared line. J Offshore Mech Arct Eng 2021;143(6):062003.
[12] Liang G, Jiang Z, Merz K. Influence of aerodynamic loads on a dual-spar floating offshore wind farm with a shared line in parked conditions. In: International conference on offshore mechanics and arctic engineering. American Society of Mechanical Engineers; 2022.
[13] Liang G, Jiang Z, Merz K. Dynamic analysis of a dual-spar floating offshore wind farm with shared moorings in extreme environmental conditions. Mar Struct 2023;90:103441.
[14] SINTEF Ocean. SIMO 4.16.0 user guide. Trondheim, Norway; 2019.
[15] SINTEF Ocean. RIFLEX 4.16.0 user guide. Trondheim, Norway; 2019.
[16] Liang G, Hanssen FCW, Merz KO, Jiang Z. Numerical analysis of a tethered-buoy mooring system for a prototype floating wind farm. 2024, http://dx.doi.org/10.1002/WE.2898, Accepted by Wind Energy.
[17] Nielsen FG, Hanson TD, Skaare B. Integrated dynamic analysis of floating offshore wind turbines. In: International conference on offshore mechanics and arctic engineering. volume 47462, 2006, p. 671–9.
[18] Duan F, Hu Z, Niedzwecki J. Model test investigation of a spar floating wind turbine. Mar Struct 2016;49:76–96.
[19] Xu X, Day S. Experimental investigation on dynamic responses of a spar-type offshore floating wind turbine and its mooring system behaviour. Ocean Eng 2021;236:109488.
[20] Roddier D, Cermelli C, Aubault A, Weinstein A. WindFloat: A floating foundation for offshore wind turbines. J Renew Sustain Energy 2010;2(3):033104.
[21] Jessen K, Laugesen K, M. Mortensen S, K. Jensen J, N. Soltani M. Experimental validation of aero-hydro-servo-elastic models of a scaled floating offshore wind turbine. Appl Sci 2019;9(6):1244.
[22] Equinor ASA. Hywind Scotland - the world's first floating wind farm. 2022, URL https://www.equinor.com/energy/hywind-scotland, [Accessed Nov. 21, 2022].
[23] Equinor ASA. Hywind Tampen: the world's first renewable power for offshore oil and gas. 2022, URL https://www.equinor.com/energy/hywind-tampen, [Accessed Nov. 21, 2022].
[24] Lopez-Olocco T, González-Gutiérrez LM, Calderon-Sanchez J, Marón Loureiro A, Saavedra Ynocente L, Bezunartea Barrio A, Vivar Valdés N. Experimental and numerical study of the influence of clumped weights on a scaled mooring line. J Mar Sci Eng 2022;10(5):676.
[25] Jonkman J, Butterfield S, Musial W, Scott G. Definition of a 5-MW reference wind turbine for offshore system development. Golden, CO, USA: NNational Renewable Energy Laboratory; 2009, NREL/TP-500-38060.
[26] Jonkman J. Definition of the floating system for phase IV of OC3. Golden, CO, USA: National Renewable Energy Laboratory; 2010, NREL/TP-500-47535.
[27] Barthelmie RJ, Jensen L. Evaluation of wind farm efficiency and wind turbine wakes at the nysted offshore wind farm. Wind Energy 2010;13(6):573–86.
[28] Lopez-Olocco T, Liang G, Medina-Manuel A, Ynocente LS, Jiang Z, Souto-Iglesias A. Experimental comparison of a dual-spar floating wind farm with shared mooring against a single floating wind turbine under wave conditions. Eng Struct 2023;292:116475.
[29] DNV. SESAM user manual, WADAM, wave analysis by diffraction and morison theory. Høvik, Norway; 2019.
[30] Irvine H. Cable structures. Dover Publications; 1992.
[31] Skaare B, Nielsen FG, Hanson TD, Yttervik R, Havmøller O, Rekdal A. Analysis of measurements and simulations from the Hywind Demo floating wind turbine. Wind Energy 2015;18(6):1105–22.
[32] Chakrabarti SK. Offshore structure modeling, vol. 9, World Scientific; 1994.
[33] Journée JM, Massie W. Offshore hydromechanics, vol. 1, Delft University of Technology Delft; 2001.
[34] Bergdahl L, Palm J, Eskilsson C, Lindahl J. Dynamically scaled model experiment of a mooring cable. J Mar Sci Eng 2016;4(1):5.
[35] Barrera C, Guanche R, Losada IJ. Experimental modelling of mooring systems for floating marine energy concepts. Mar Struct 2019;63:153–80.
[36] Northern Digital Inc. Optotrak certus. 2022, URL https://www.ndigital.com/products/legacy-products/, [Accessed Nov. 21, 2022].
[37] Li L, Gao Z, Moan T. Joint distribution of environmental condition at five European offshore sites for design of combined wind and wave energy devices. J Offshore Mech Arct Eng 2015;137(3).
[38] DNV. Recommended practice DNV-RP-C205, Environmental conditions and environmental loads. Høvik, Norway; 2010.
[39] ITTC. Recommended procedures and guidelines: Model tests for offshore wind turbines. 2017.
[40] ITTC. Recommended procedures and guidelines: Floating offshore platform experiments. 2017.
[41] ITTC. Recommended procedures and guidelines: Testing and extrapolation methods loads and responses, stability model tests on intact stability. 2008.
[42] Faltinsen O. Sea loads on ships and offshore structures, vol. 1, Cambridge University Press; 1993.
[43] Ikhennicheu M, Lynch M, Doole S, Borisade F, Matha D, Dominguez J, Vicente R, Tim H, Ramirez L, Potestio S, Molins C, Trubat P. Review of the state of the art of mooring and anchoring designs, technical challenges and identification of relevant DLCs. Corewind; 2021.
[44] ABS. Guidance notes on global performance analysis for floating offshore wind turbines. Houston (TX), USA: The American Bureau of Shipping; 2020.
[45] Hsu W-t, Thiagarajan KP, Manuel L. Extreme mooring tensions due to snap loads on a floating offshore wind turbine system. Mar Struct 2017;55:182–99.
[46] DNV. Offshore standard DNV-OS-E301, Position mooring. Høvik, Norway; 2015.
[47] DNV. Recommended practice DNV-RP-0286, coupled analysis of floating wind turbines. Høvik, Norway; 2019.
[48] Lu YJ, Chen Y-N, Tan P-L, Bai Y. Prediction of most probable extreme values for jackup dynamic analysis. Mar Struct 2002;15(1):15–34.